



PERGAMON

Available online at [www.sciencedirect.com](http://www.sciencedirect.com)

SCIENCE @ DIRECT®

International Journal of Mechanical Sciences 45 (2003) 325–358

International Journal of  
MECHANICAL  
SCIENCES

[www.elsevier.com/locate/ijmesci](http://www.elsevier.com/locate/ijmesci)

# A continuum sensitivity method for the design of multi-stage metal forming processes

Nicholas Zabaras\*, Shankar Ganapathysubramanian, Qing Li

*Materials Process Design and Control Laboratory, Sibley School of Mechanical and Aerospace Engineering, 188 Frank H.T. Rhodes Hall, Cornell University, Ithaca, NY 14853-3801, USA*

Received 12 November 2002; received in revised form 5 March 2003; accepted 6 March 2003

---

## Abstract

A novel, efficient and mathematically rigorous continuum based sensitivity method is introduced that can be used to accurately evaluate the gradients of the objective function and constraints in the optimization-based design of multi-stage deformation processes. Weak sensitivity equilibrium equations are derived for the large deformation of the workpiece in each forming operation. This sensitivity kinematic problem is linearly coupled with the corresponding continuum sensitivity constitutive, contact and thermal sub-problems for the particular process. Thus a linear sensitivity problem with appropriate driving forces is identified and the analysis is carried out in an infinite dimensional framework. The multi-stage continuum sensitivity analysis takes a form similar to the updated Lagrangian sensitivity framework developed earlier for the design of single-stage deformation processes. It allows us to treat in a unified manner shape and parameter sensitivity analyses that are both present in a typical design problem of multi-stage deformation processes. The effectiveness of the proposed methodology is demonstrated with the solution of three practical problems in the design of two-stage metal forming processes.

© 2003 Elsevier Science Ltd. All rights reserved.

*Keywords:* Computational design; Materials process design; Multi-stage deformation processing; Metal forming; Sensitivity analysis

---

## 1. Introduction

In spite of the increased use of computer technology in the analysis of deformation processes, selection of actual process design variables (number of different dies, shapes of dies and preforms, etc.) still requires a significant amount of expert knowledge that is commonly obtained only through experience. To overcome this dependency on a small group of industry experts and to reach robust

---

\* Corresponding author. Tel.: +1-607-255-9104; fax: +1-607-255-9410.

E-mail address: [zabaras@cornell.edu](mailto:zabaras@cornell.edu) (N. Zabaras).

## Nomenclature

|   |  |
|---|--|
| $\mathcal{B}_0$                                 | reference configuration for design differentiation (time $t = 0$ )                   |
| $\mathcal{B}_0^c \equiv \mathcal{B}_f^h$        | initial preform at the current stage $t = t_f^h$                                     |
| $\mathcal{B}_{n+1}^c$                           | current configuration at time $t_{n+1}^c$  |
| $\mathcal{B}_n^c$                               | reference configuration in the updated Lagrangian analysis                           |
| $\mathbf{F}_r$                                  | deformation gradient at $\mathcal{B}_{n+1}^c$ with respect to $\mathcal{B}_n^c$      |
| $\mathbf{F}_{n+1}$                              | deformation gradient at $\mathcal{B}_{n+1}^c$ with respect to $\mathcal{B}_0^c$      |
| $\mathbf{F}_{n+1}^c$                            | deformation gradient at $\mathcal{B}_{n+1}^c$ with respect to $\mathcal{B}_0$        |
| $\mathbf{F}^e, \mathbf{F}^p, \mathbf{F}^\theta$ | elastic, plastic and thermal parts of $\mathbf{F}_{n+1}^c$                           |
| $\mathbf{F}^{vol}, \mathbf{F}^{dev}$            | volumetric and deviatoric components of $\mathbf{F}_r$                               |
| $\bar{\mathbf{F}}_h$                            | assumed-strain discretized relative gradient $\mathbf{F}_r$                          |
| $\bar{\mathbf{F}}_h^{ave}$                      | average relative gradient $\mathbf{F}_r$ (Eq. (2.21))                                |
| $\mathcal{G}(\mathbf{x})$                       | gap function at the point $\mathbf{x}$   |
| $\mathbf{L}_n^c$                                | design velocity gradient at $t_n^c$  |
| $\mathcal{L}^e$                                 | elastic moduli   |
| $\mathbf{N}$                                    | unit normal vector to $\Gamma_n^c$   |
| $\mathbf{P}_r$                                  | Piola–Kirchhoff I stress in $\mathcal{B}_{n+1}^c$ per unit area of $\mathcal{B}_n^c$ |
| $\mathcal{Q}_n^c$                               | collection of $(\mathbf{F}^p, s, \theta)$ in the configuration $\mathcal{B}_n^c$     |
| $s$   | isotropic scalar state variable  |
| $\mathbf{T}$                                    | cauchy stress in $\mathcal{B}_{n+1}^c$   |
| $\mathcal{W}_{mech}$                            | mechanical dissipation in the workpiece  |
| $\mathbf{Y}, \mathbf{X}, \mathbf{x}_n$          | material particle location in $\mathcal{B}_0, \mathcal{B}_0^c, \mathcal{B}_n^c$      |
| $\beta^c$                                       | collection of design variables in the current forming stage                          |
| $\beta^h$                                       | collection of design variables in earlier forming stages                             |
| $\beta$   | coefficient of thermal expansion   |
| $\varepsilon_N, \varepsilon_T$                  | normal/tangential sensitivity contact penalty numbers                                |
| $\theta$  | temperature in the workpiece   |
| $\lambda_T, \lambda_N$                          | normal/tangential tractions per unit area of $\mathcal{B}_n^c$                       |
| $\Phi$  | arbitrary Lagrangian field   |
| $\overset{\circ}{\Phi}$                         | gateaux differential of $\Phi$   |
| $\phi_i$  | basis functions in the parametric representation of dies                             |

and less costly designs, reliable optimization-based design techniques for plastic deformation are being developed.

The complexity of metal forming design is apparent considering the coupled non-linear physical mechanisms that need to be accounted for such as (a) large deformation plasticity, (b) deformation induced microstructure evolution, (c) time varying contact and friction conditions, (d) thermal effects and mechanical dissipation and (e) damage accumulation leading to material rupture. The role of these mechanisms in the processing of the initial workpiece to yield the final product is

paramount. Metal forming process design therefore requires the accurate description and control of these deformation mechanisms.

There are many factors that result in poor material utilization rates, high cost of process equipment and lack of complete control on final product quality, in fact, so many that it is impossible for a non-expert designer to simultaneously consider all of them while making decisions. Design objectives may vary from process to process and multi-objective designs for the same process are common. One typically desires the simultaneous satisfaction of one or more of the competing criteria defined in Box 1.

Box 1. Objectives in hot forming design.

- Minimization of material usage
- Uniform deformation in the final product
- Minimum required work or forming force
- Desired microstructure in the final product
- Minimum or desired residual stress distribution
- Minimum deformation and wear of the die
- Desired shape of the final product
- Minimum porosity in the final product

The design process is often subject to various processing constraints including maximum available press load capacity and press speeds, windows of processing temperatures and strain rates, final product quality, cost and others. In industrial forming applications, the objectives indicated in Box 1 are seldom simple enough to be achieved by a single forming operation. As a result, intermediate deformation or preforming steps are used to efficiently transform the initial geometry into a final shape with desired material properties. A forming sequence can be viewed at two levels for the purpose of design: (1) the broad identification of the number, type and order of forming and heat-treatment operations that make up the sequence (e.g. forward extrusion, open die forging) and (2) the specific identification and selection of design variables in each of the forming operations (e.g. ram speed and die stroke, lubrication conditions, die and preform shapes, operating temperature conditions, etc.). A schematic of a simple forging sequence depicting the process of uniformly increasing the cross section of an initial round bar stock is shown in Fig. 1. Such design problems were introduced and examined by Kobayashi and colleagues using the backward tracing technique [1].

In this paper, we will address the development of a mathematically and computationally rigorous gradient-based optimization methodology for a virtual materials process design that is based on quantified product quality and accounts for process targets and constraints. The virtual design simulator depicted in Box 2 includes the development of a sensitivity analysis consistent to a virtual direct process simulator that is capable of accurately computing the gradients of objective functions and process constraints.

The use of sensitivity analysis to address deformation design problems is recently receiving extensive attention [2]. Sensitivities can be computed either by employing finite differences (FDM), direct differentiation (DDM) or the adjoint variable method [3]. In the DDM method, one solves

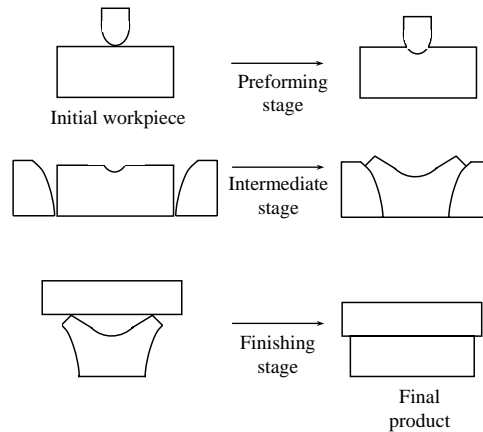


Fig 1. Schematic of a multi-stage forging sequence depicting the process of uniformly increasing the cross section of an initial round bar stock.

#### Box 2. A computational design simulator for forming processes.

- Mathematical representation of the design objective
- Selection of the sequence of processes (stages) and initial process parameter designs using knowledge based expert systems, microstructure evolution paths and/or ideal forming techniques
- Selection of the design variables (e.g. parametric representation of dies/preforms)
- Selection of a virtual direct process model
- Interactive optimization environment
- Continuum multi-stage process sensitivity analysis consistent with the direct process model
- Optimization algorithms
- Assessment of automatic process optimization
- Reliability of the optimal design to physical and computational model errors

for the response sensitivities simultaneously with the solution of the direct deformation problem. On the other hand, the FDM involves an additional solution of the direct deformation problem for a perturbed set of design parameters. The DDM method is chosen in this paper as the preferred method for evaluating sensitivities in deformation processing. Different schemes of design differentiation can be envisioned depending on the level at which the design differentiation is performed. In our earlier work, the equations governing the sensitivity fields were computed at the continuum level [4]. In an alternate discrete sensitivity description, the sensitivity equations are derived by design differentiation of their discrete counterparts in the direct problem [5,6]. The final scheme refers to the differentiation of the direct deformation simulator at the level of the numerical code [7].

Most of the developments in the sensitivity analysis of metal forming processes use the flow formulation and are limited to steady state applications [8]. A sensitivity analysis of non-steady state

deformations using the solid formulation and small deformation elasto-plasticity theory can be found in Ref. [9]. Additional work on optimization of metal forming processes using a gradient based approach and a flow FEM formulation is given in Refs. [10–15]. The limited number of publications in multi-stage forming process design include [16,17].

A framework for preform as well as process parameter optimization is proposed here for multi-stage metal forming processes. The design of each individual process will be performed using gradient-optimization techniques that are based on a rigorous continuum sensitivity method (CSM). Multi-stage sensitivity algorithms are proposed that allow the sensitivity fields of individual processes to be used in multi-stage process design. Optimal microstructure evolution paths, ideal forming techniques [18,19] and knowledge based expert systems techniques [20–23] can be developed to select the required sequence of processes and to develop feasible initial designs. However, in the work reported here, the required sequence of processes is a priori selected to allow us to concentrate in the development of the CSM for multi-stage processes.

In this paper, we extend the continuum sensitivity method developed by Zabaras and colleagues for single-stage deformation processes [4,24–26] to compute the sensitivities of non-isothermal multi-stage forming processes using an updated Lagrangian approach. Our earlier attempts to model multi-stage forming processes are reported in Ref. [27] where two-stage isothermal forming processes are discussed using a total Lagrangian analysis that was only effective for forming processes with simple workpiece geometries that do not require remeshing and subsequent data transfer operations. Sensitivity analysis of a multi-stage process necessarily involves the computation of both shape as well as parameter sensitivities. However, unlike single-stage shape sensitivity analysis where the initial workpiece shape depends explicitly on shape design variables, the intermediate preform shape in a generic forming stage of a multi-stage process depends implicitly on the design variables (non-shape parameters) that define the processing history of the intermediate preform. It will be shown that the computation of parameter and shape sensitivities in a single stage process as reported in Refs. [25,26] are specific cases of the generic developments described here. To the authors best knowledge, this is the first time that such a rigorous and accurate sensitivity analysis has been developed and implemented for multi-stage forming processes.

The sequencing of the various sections in the paper is as follows. The kinematic and constitutive equations and contact/frictional laws pertinent to the direct multi-stage deformation analysis are reviewed in Section 2. The continuum sensitivity method for a multi-stage deformation process is introduced in Section 3. The CSM method for shape or parameter analysis for each deformation stage is an essential ingredient of the multi-stage sensitivity analysis and is reviewed in Section 4. Section 5 presents a number of two-stage design examples together with a discussion on the accuracy and efficiency of the multi-stage CSM method. The paper concludes with Section 6 that provides a summary of this work and a discussion of pending research issues in multi-stage forming design.

## 2. Direct analysis of a forming sequence

Fig. 2 presents the various material configurations through which the workpiece underwent in its processing history as well as the configurations obtained in the current processing step. Let us denote with  $\mathcal{B}_0$  the initial virgin configuration of the body before any processing and with  $\mathcal{B}_f^h$  the final

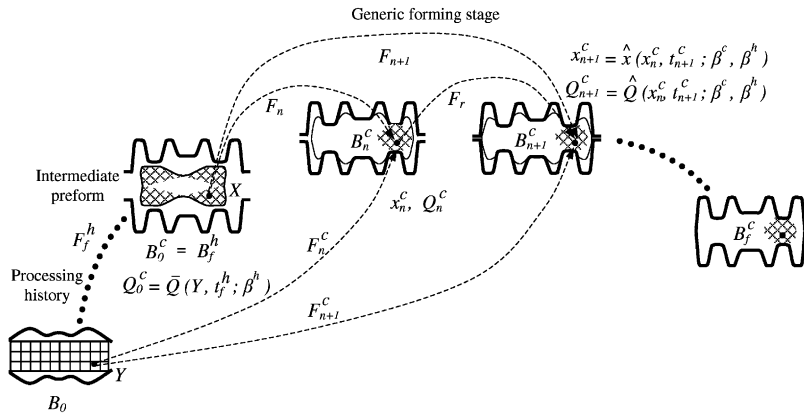


Fig 2. Schematic of an updated Lagrangian framework for a multi-stage deformation process. The superscript *c* refers to the current stage, whereas the superscript *h* refers to the deformation processing history. The configuration  $\mathcal{B}_n^c$  is used as the reference configuration in computing the configuration  $\mathcal{B}_{n+1}^c$  and the set  $\mathcal{Q}_{n+1}^c$ , where  $\mathcal{Q} = \{\mathbf{F}^p, s, \theta\}$ .

configuration obtained at time  $t_f^h$  as a result of the processing history. This configuration is the same as the initial configuration  $\mathcal{B}_0^c$  (time  $t_0^c \equiv t_f^h$ ) in the current processing stage.

The direct problem can be stated as follows: Compute the time history of the deformation, temperature, material state and plastic deformation of a body deforming as a result of external forces and/or deformation due to contact and friction at the workpiece-die interface. The deformation problem is sub-divided into kinematic, constitutive, contact and thermal sub-problems. An updated Lagrangian FEM formulation is used to solve the direct deformation problem in a generic forming stage in which material occupying an initial configuration (intermediate preform)  $\mathcal{B}_0^c$  ( $t = t_0^c$ ) is deformed to obtain a final configuration (final preform)  $\mathcal{B}_f^c$  ( $t = t_f^c$ ). To compute the material configuration  $\mathcal{B}_{n+1}^c$  (from now on called the current configuration) for  $n=0, 1, \dots, (f-1)$ , we proceed in an incremental fashion using the configuration  $\mathcal{B}_n^c$  as the reference configuration.

Let  $\mathbf{Y}$  be a material particle in  $\mathcal{B}_0$  and let  $\mathbf{X}$  be its location in the configuration  $\mathcal{B}_0^c$  as a result of the processing history. The location of the particle  $\mathbf{Y}$  in the current processing stage is defined with the mapping

$$\mathbf{x}^c = \bar{\mathbf{x}}(\mathbf{Y}, t) = \tilde{\mathbf{x}}(\mathbf{X}, t) = \hat{\mathbf{x}}(\mathbf{x}_n^c, t), \quad t \in [t_n^c, t_{n+1}^c], \tag{2.1}$$

where  $\mathbf{x}_n^c$  is the particle location in the reference configuration  $\mathcal{B}_n^c$ . Note that the particle  $\mathbf{Y}$  is defined in the initial configuration  $\mathcal{B}_0$  before any deformation is initiated (Fig. 2). Using an updated Lagrangian framework, one introduces the deformation gradient  $\mathbf{F}_r$  with respect to the reference configuration  $\mathcal{B}_n^c$  and expresses the total (with respect to the virgin configuration  $\mathcal{B}_0$ ) deformation gradient  $\mathbf{F}_{n+1}^c$  at time  $t = t_{n+1}^c$  as follows:

$$\mathbf{F}_{n+1}^c = \frac{\partial \bar{\mathbf{x}}(\mathbf{Y}, t_{n+1}^c)}{\partial \mathbf{Y}} = \nabla_n \hat{\mathbf{x}}(\mathbf{x}_n^c, t_{n+1}^c) \frac{\partial \bar{\mathbf{x}}(\mathbf{Y}, t_n^c)}{\partial \mathbf{Y}} = \mathbf{F}_r \mathbf{F}_n^c. \tag{2.2}$$

In the following equations, all additional field variables introduced that are defined in the current configuration  $\mathcal{B}_{n+1}^c$  (time  $t = t_{n+1}^c$ ) will be denoted without using the subscript  $n+1$  and superscript *c*.

In an appropriate kinematic framework for large deformation inelastic analysis including thermal effects, the total deformation gradient is decomposed into thermal, plastic and elastic parts as follows:

$$\mathbf{F} \equiv \mathbf{F}_{n+1}^c = \mathbf{F}^e \mathbf{F}^p \mathbf{F}^\theta, \tag{2.3}$$

where  $\mathbf{F}^e$  is the elastic deformation gradient,  $\mathbf{F}^p$ , the plastic deformation gradient and  $\mathbf{F}^\theta$  is the thermal part of the deformation gradient in  $\mathcal{B}_{n+1}^c$ . With the above constitutive framework, notions of an intermediate thermally expanded hot unstressed configuration and of an intermediate hot plastically deformed relaxed configuration are introduced [28]. Assuming isotropic thermal expansion, the evolution of the intermediate thermally expanded unstressed configuration is given as follows:

$$\dot{\mathbf{F}}^\theta \mathbf{F}^{\theta-1} = \beta \dot{\theta} \mathbf{I}, \tag{2.4}$$

where  $\mathbf{I}$  is the second-order identity tensor and  $\beta$  the thermal expansion coefficient.

Following Anand [29], the hyperelastic constitutive equations are written as

$$\bar{\mathbf{T}} = \mathcal{L}^e[\bar{\mathbf{E}}^e], \tag{2.5}$$

where the strain measure,  $\bar{\mathbf{E}}^e$ , is defined with respect to the intermediate (unstressed) configuration as  $\bar{\mathbf{E}}^e = \ln \mathbf{U}^e$ . The corresponding conjugate stress measure  $\bar{\mathbf{T}}$  is the pullback of the Kirchhoff stress with respect to  $\mathbf{R}^e$ ,

$$\bar{\mathbf{T}} = \det(\mathbf{U}^e) \mathbf{R}^{eT} \mathbf{T} \mathbf{R}^e. \tag{2.6}$$

Here  $\mathbf{U}^e$  and  $\mathbf{R}^e$  are calculated from the polar decomposition  $\mathbf{F}^e = \mathbf{R}^e \mathbf{U}^e$ . For an isotropic material, the elastic moduli  $\mathcal{L}^e$  are given by

$$\mathcal{L}^e = 2\mu \mathcal{J} + \left( \kappa - \frac{2}{3}\mu \right) \mathbf{I} \otimes \mathbf{I}, \tag{2.7}$$

where  $\mu$  is the shear modulus,  $\kappa$  is the bulk modulus and  $\mathcal{J}$  denotes the unit fourth order tensor.

The equilibrium equation at  $t = t_{n+1}^c$  can be expressed in the reference configuration  $\mathcal{B}_n^c$  as,

$$\nabla_n \cdot \mathbf{P}_r + \mathbf{f} = \mathbf{0}, \tag{2.8}$$

where  $\nabla_n \cdot$  denotes the divergence in  $\mathcal{B}_n^c$ . The Piola–Kirchhoff I stress  $\mathbf{P}_r$  is expressed per unit area of  $\mathcal{B}_n^c$  and given as follows:

$$\mathbf{P}_r = \det \mathbf{F}_r \mathbf{T} \mathbf{F}_r^{-T}. \tag{2.9}$$

The solution of the deformation problem in the current processing stage proceeds incrementally in time starting from the initial configuration  $\mathcal{B}_0^c$ . In order to solve the equilibrium Eq. (2.8) at time  $t = t_{n+1}^c$ , the constitutive relationship between the Cauchy stress  $\mathbf{T}$  and the relative deformation gradient  $\mathbf{F}_r$  and temperature  $\theta$  should be evaluated. This is discussed in detail in Refs. [28,30]. A hyperelastic–viscoplastic constitutive framework is used here and the evolution of  $\mathbf{F}^p$  is modeled using the classical  $J_2$  flow theory with a single scalar state variable  $s$ . The evolution of the plastic deformation gradient  $\mathbf{F}^p$  is given by the normality rule as follows:

$$\bar{\mathbf{L}}^p = \dot{\mathbf{F}}^p \mathbf{F}^{p-1}, \tag{2.10}$$

where  $\bar{\mathbf{L}}^p = \bar{\mathbf{D}}^p$  and  $\bar{\mathbf{W}}^p = \mathbf{0}$ .

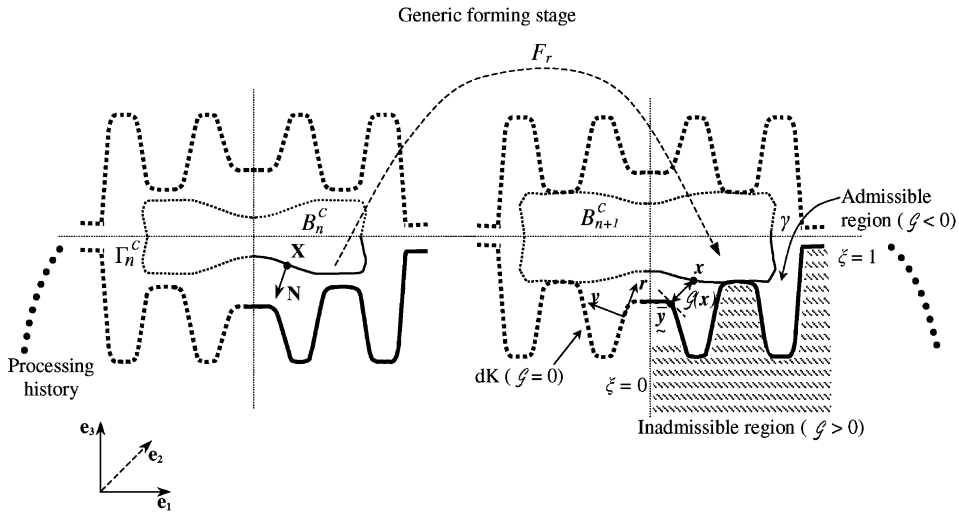


Fig 3. A schematic of the contact sub-problem in a generic forming stage showing the definition of the gap function, of the admissible and inadmissible regions.

The flow rule can be stated as,

$$\bar{D}^p = \sqrt{\frac{3}{2}} \frac{\dot{\tilde{\epsilon}}^p \bar{T}'}{\|\bar{T}'\|}. \tag{2.11}$$

The evolution of the equivalent tensile plastic strain is specified via uniaxial experiments as

$$\dot{\tilde{\epsilon}}^p = f(\tilde{\sigma}, s, \theta) \tag{2.12}$$

and the evolution of the isotropic scalar resistance  $s$  is also obtained from experiments and has the form

$$\dot{s} = g(\tilde{\sigma}, s, \theta) = h(\tilde{\sigma}, s, \theta) \dot{\tilde{\epsilon}}^p - \dot{r}(s, \theta), \tag{2.13}$$

where  $\dot{r}(s, \theta)$  is the static recovery function and  $\tilde{\sigma}$  the equivalent stress. A radial return type algorithm is used to solve the above constitutive problem.

Contact and friction is modeled following the scheme suggested in Refs. [31,32]. A schematic of the contact problem is shown in Fig. 3. The parametric representation of the die  $\mathcal{D}$  is introduced in two dimensions using a parameter  $\xi$  and the function  $y(\xi)$ ,  $0 \leq \xi \leq 1$ . A fixed right-handed basis  $(e_1, e_2, e_3)$  is considered and a convected basis  $(r, e_2, v)$  is defined at each point for a particular value of  $\xi$ . The tangent vector  $\tau_1$  and the unit tangent vector  $r$  are given by

$$\tau_1 = y_{,\xi} \quad r = \frac{\tau_1}{\|\tau_1\|} \tag{2.14}$$

The die separates the space into admissible and inadmissible regions and  $\Gamma_n^c \subset \partial B_n^c$  refers to the part of the boundary that could potentially come in contact. We define the gap function  $\mathcal{G}$  of any point  $x$  in space as the shortest distance of that point from the die:

$$\bar{y} - x = \mathcal{G}(x)v(\bar{y}), \tag{2.15}$$

where  $\bar{\mathbf{y}} \in \mathcal{D}$  is the value of  $\mathbf{y}$  that minimizes the norm  $\|\mathbf{x} - \mathbf{y}\|$ . With this definition of the gap function, the impenetrability constraints are given as follows: For all  $\mathbf{x}_n^c \in \Gamma_n^c$ , with  $\mathbf{x}_{n+1}^c = \hat{\mathbf{x}}(\mathbf{x}_n^c, t_{n+1}^c)$

$$\begin{aligned} \mathcal{G}(\mathbf{x}_{n+1}^c) &\leq 0, \\ \lambda_N &= \mathbf{v} \cdot \boldsymbol{\lambda}, \\ \lambda_N \mathcal{G}(\mathbf{x}_{n+1}^c) &= 0, \end{aligned} \tag{2.16}$$

where  $\lambda_N$  is the absolute value of the contact pressure. The vector  $\boldsymbol{\lambda}$  is the current traction per unit area in  $\Gamma_n^c \in \partial \mathcal{B}_n^c$ . The Coulomb friction law can be written as

$$\begin{aligned} \boldsymbol{\lambda}_T &= -\boldsymbol{\lambda} + \lambda_N \mathbf{v}, \\ \mathcal{T} &:= \|\boldsymbol{\lambda}_T\| - \mu \lambda_N \leq 0, \\ \mathbf{v}_T &= \chi \frac{\boldsymbol{\lambda}_T}{\|\boldsymbol{\lambda}_T\|}, \\ \chi &\geq 0, \\ \chi \mathcal{T} &= 0, \end{aligned} \tag{2.17}$$

where  $\boldsymbol{\lambda}_T$  is the tangential contact traction vector,  $\mu$  is the Coulomb friction coefficient and  $\mathcal{T}$  is the slip function.

The solution of a generic loading increment at  $t = t_{n+1}^c$  includes the solution to the principle of virtual work (PVW) given as follows:

$$\int_{\mathcal{B}_n^c} \mathbf{P}_r(\mathbf{F}_r) \cdot \nabla_n \tilde{\mathbf{u}} \, dV_n^c = \int_{\Gamma_n^c} \boldsymbol{\lambda} \cdot \tilde{\mathbf{u}} \, dA_n^c + \int_{\mathcal{B}_n^c} \mathbf{f} \cdot \tilde{\mathbf{u}} \, dV_n^c \tag{2.18}$$

for every admissible test function  $\tilde{\mathbf{u}}$  expressed over the reference configuration  $\mathcal{B}_n^c$ . The above weak form is solved in an incremental-iterative manner as a result of the material and geometric non-linearities.

The FEM is used for the solution of the weak form using the standard bilinear quadrilateral element with four Gauss integration points. Since this element performs poorly in the incompressible limit exhibiting an excessively stiff locking response, the  $\mathbf{F}$ -bar method with an a priori stabilization factor has been implemented [33]. The continuum deformation gradient  $\mathbf{F}_r$  with respect to the reference configuration  $\mathcal{B}_n^c$  admits the following volumetric–deviatoric decomposition:

$$\begin{aligned} \mathbf{F}_h &= \mathbf{F}^{vol} \mathbf{F}^{dev}, \\ \mathbf{F}^{vol} &= J^{\frac{1}{3}} \mathbf{I}, \\ \mathbf{F}^{dev} &= J^{-\frac{1}{3}} \mathbf{F}_r, \\ J &= \det(\mathbf{F}_r). \end{aligned} \tag{2.19}$$

Let  $\mathbf{F}_h$  be the discrete FEM-compatible counterpart of  $\mathbf{F}_r$ . In the context of the assumed strain analysis, a discrete representation  $\bar{\mathbf{F}}_h$  of  $\mathbf{F}_r$  in a typical finite element is also introduced as

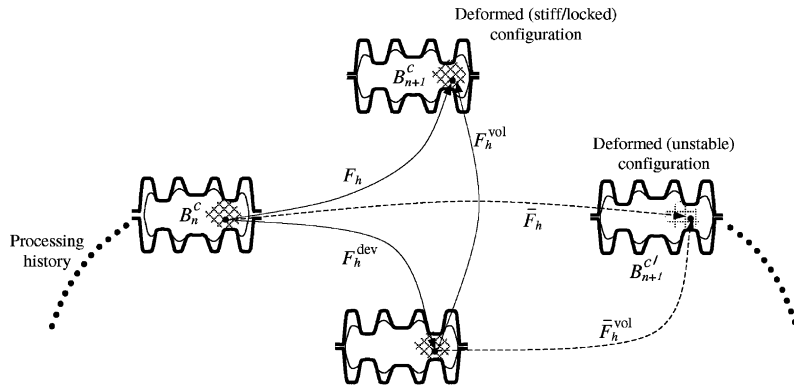


Fig 4. A schematic of the volumetric–deviatoric multiplicative decomposition used in the finite element model of the deformation. An  $\varepsilon$ -weighted average of  $\mathcal{B}_{n+1}^c$  and  $\mathcal{B}_{n+1}^{c'}$  is selected as the admissible discretized configuration at  $t_{n+1}^c$ .

follows:

$$\begin{aligned} \bar{\mathbf{F}}_h &= \bar{\mathbf{F}}_h^{vol} \mathbf{F}_h^{dev}, \\ \bar{\mathbf{F}}_h^{vol} &= \bar{J}_h^{1/3} \mathbf{I} = \left[ \sum_{a=1}^{\overline{NINT}} J_{ha}(\bar{\xi}_a) \bar{N}_a \right]^{1/3} \mathbf{I} \\ \mathbf{F}_h^{dev} &= J_h^{-1/3} \mathbf{F}_h \end{aligned} \tag{2.20}$$

where  $\bar{\xi}_a$ ,  $a = 1, \dots, \overline{NINT}$  represent the reduced quadrature points and  $\bar{N}_a$  are the extrapolation (bar) shape functions such that  $\bar{N}_a(\bar{\xi}_b) = \delta_{ab}$ . A schematic of this decomposition is shown in Fig. 4. The use of a pre-determined number of volumetric degrees of freedom circumvents the issue of locking in nearly-incompressible deformations. However, this reduced integration leads to hour-glass instabilities in the deformation pattern [34]. In order to obtain a stable solution, an a priori stabilization method which introduces an empirical (small, positive) scalar parameter  $\varepsilon \rightarrow 0$ , is used to define the assumed deformation gradient as

$$\mathbf{F}_h^{ave} \equiv \varepsilon \mathbf{F}_h + (1 - \varepsilon) \bar{\mathbf{F}}_h. \tag{2.21}$$

In the  $\mathbf{F}$ -bar method, only the constitutive response is modified. Thus  $\mathbf{P}_r \equiv \mathbf{P}_r(\mathbf{F}_h^{ave})$  is used in the finite element representation of the internal work term in Eq. (2.18), i.e.

$$\mathcal{G}_h^{int} \equiv \sum_e \int_{\Omega_e} \mathbf{P}_r(\mathbf{F}_h^{ave}) \cdot \nabla_n \tilde{\mathbf{u}}_h \, dV_n^c \tag{2.22}$$

Let us now consider the mechanics in-between two forming stages. This phase usually consists of an unloading process where one of the dies is removed from contact with the workpiece. The unloading process is modeled as a non-linear (finite deformation) elasto-static boundary value problem. If  $\mathcal{B}$  represents the final configuration of the workpiece at the end of the loading phase with the total deformation gradient given as  $\mathbf{F} = \mathbf{F}^e \mathbf{F}^p \mathbf{F}^\theta$ , then the solution to the unloading process results in the final body configuration  $\mathcal{B}_u$  with the total deformation gradient given as  $\mathbf{F}_u = \mathbf{F}_u^e \mathbf{F}_u^p \mathbf{F}_u^\theta$ . The modeling

of the unloading phase (residual stresses) can be quite significant in the design of forgings with thin sections where residual stresses cause significant warpage. The workpiece material also undergoes a recovery process, whereby the material state evolves in the absence of an applied stress. The duration in-between forming stages is therefore characterized by the evolution of the inelastic internal variable  $s$  as a result of varying temperature distribution in the workpiece. In this work, the static recovery function  $\dot{r}$  in Eq. (2.13) is taken as zero and the forming stages proceed from one stage to another stage immediately upon completion of the unloading process.

### 3. The continuum sensitivity method for multi-stage processes

In this section, we introduce notions of the sensitivity of various physical fields with respect to small changes in the design variables of the forming sequence given in Fig. 2. Let  $\beta^h$  be a set of design parameters that define the processing history (deformation from  $\mathcal{B}_0$  to  $\mathcal{B}_f^h \equiv \mathcal{B}_0^c$ ). These parameters can represent various preform shapes in this processing history and/or various process parameters such as die surfaces, ram speed time histories, and others. The deformation history leading to the intermediate preform  $\mathcal{B}_0^c$  for each selection of the design variables  $\beta^h$  is thus described as follows:

$$X = \bar{x}(Y, t_f^h; \beta^h), \quad \forall Y \in \mathcal{B}_0, \tag{3.1}$$

$$Q_0^c = \bar{Q}_0^c(Y, t_f^h; \beta^h), \quad \forall Y \in \mathcal{B}_0, \tag{3.2}$$

where  $Q = \{F^p, s, \theta\}$  is introduced to characterize the minimum set of field variables needed to define each deformation stage.

With a given configuration  $\mathcal{B}_0^c$  and field variables  $Q_0^c$  (i.e. for a given  $\beta^h$ ), the configurations  $\mathcal{B}_i^c$ ,  $i = 1, 2, \dots, f$ , of the current forming stage are completely defined through the following mappings (Fig. 2):

$$x = \tilde{x}(X, t; \beta^c) = \bar{x}(Y, t; \beta^h, \beta^c), \quad \forall X \in \mathcal{B}_0^c, \quad t \in [t_0^c, t_f^c], \tag{3.3}$$

$$Q = \tilde{Q}(X, t; \beta^c) = \bar{Q}(Y, t; \beta^h, \beta^c), \quad \forall X \in \mathcal{B}_0^c, \quad t \in [t_0^c, t_f^c], \tag{3.4}$$

where  $\beta^c$  represents the design variables (shape or parameter) in the current forming stage. The design variable set  $\beta^h \cup \beta^c$  will be denoted from now on simply as  $\beta$ .

We are interested to define and compute the sensitivity of various kinematic, thermal, plastic deformation and material state related field variables in the current forming stage with respect to the design variables  $\beta$ . As a minimum requirement for such calculations, one needs to compute the sensitivities of  $x$  and  $Q$  at each time step with respect to  $\beta$ . The sensitivity of a field variable is a quantitative measure of changes in each field as a result of infinitesimal perturbations to the parameters  $\beta$ .

Let us consider at first the sensitivities with respect to the design parameters  $\beta^c$  of field variables in the current forming stage with a fixed  $\beta^h$  (thus a given  $\mathcal{B}_0^c$  and  $Q_0^c$ ). Such typical process parameters may include the ram speed history, the die surface of the current stage, and others. Fig. 5 presents a schematic that shows the variation of the fields  $x^c$  and  $Q^c$  induced by a variation in the process parameter  $\beta^c$ . An updated Lagrangian representation is adopted here.

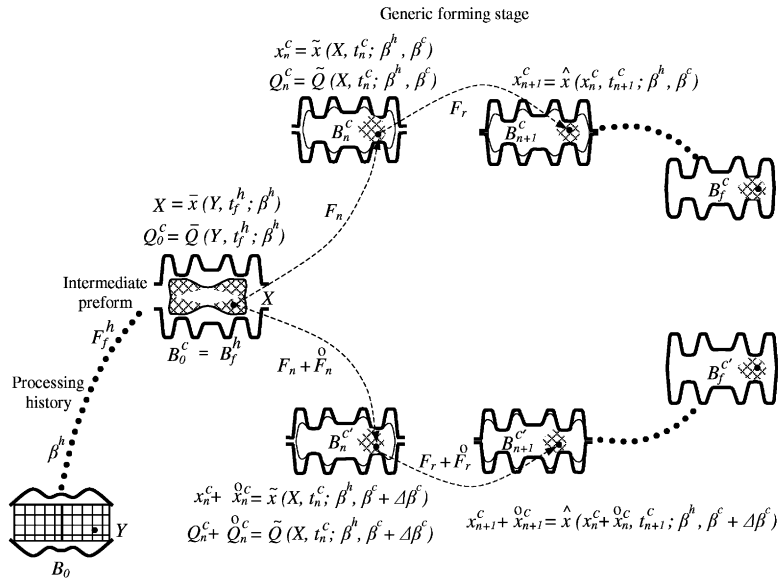


Fig 5. Schematic representation of the design sensitivity of the deformation in the current forming stage due to variations in the (non-shape) design parameters  $\beta^c$  of the current forming stage.

Let us consider a generic field  $\Phi$  that can represent  $x$ ,  $Q$  or any other material or deformation related field. The dependence of the UL field  $\Phi = \hat{\Phi}(x_n, t)$  on  $\beta^c$  can be expressed as follows:

$$\Phi = \hat{\Phi}(x_n^c, t; \beta^c) = \hat{\Phi}(\tilde{x}(X, t; \beta^c), t; \beta^c) = \tilde{\Phi}(X, t; \beta^c), \quad t \in [t_n^c, t_{n+1}^c] \tag{3.5}$$

with the position  $x_n^c$  referred to the reference configuration  $\mathcal{B}_n^c$ . The parameter sensitivity  $\overset{\circ}{\Phi} = \hat{\Phi}(x_n^c, t; \beta^c, \Delta\beta^c)$  is defined as the total Gateaux differential of  $\Phi = \hat{\Phi}(x_n^c, t; \beta^c)$  in the direction  $\Delta\beta^c$  computed at  $\beta^c$ :

$$\begin{aligned} \overset{\circ}{\Phi}(x_n^c, t; \beta^c, \Delta\beta^c) &= \overset{\circ}{\tilde{\Phi}}(X, t; \beta^c, \Delta\beta^c) \\ &= \left. \frac{d}{d\omega} \tilde{\Phi}(X, t; \beta^c + \omega\Delta\beta^c) \right|_{\omega=0}, \quad t \in [t_n^c, t_{n+1}^c]. \end{aligned} \tag{3.6}$$

The parameter sensitivity  $\overset{\circ}{\Phi}$  equivalently represents the difference between two values of the field  $\Phi$ , that result due to two different current forming processes defined by the parameters  $\beta^c + \Delta\beta^c$  and  $\beta^c$  (Fig. 5), respectively, i.e.

$$\begin{aligned} \overset{\circ}{\Phi}(x_n^c, t; \beta^c, \Delta\beta^c) &= \hat{\Phi}(\tilde{x}(X, t_n^c; \beta^c + \Delta\beta^c), t; \beta^c + \Delta\beta^c) - \hat{\Phi}(\tilde{x}(X, t_n^c; \beta^c), t; \beta^c) + O(\|\Delta\beta^c\|^2) \\ &= \tilde{\Phi}(X, t; \beta^c + \Delta\beta^c) - \tilde{\Phi}(X, t; \beta^c) + O(\|\Delta\beta^c\|^2), \quad t \in [t_n^c, t_{n+1}^c]. \end{aligned} \tag{3.7}$$

The explicit dependence of Lagrangian fields on the design parameters  $\beta^c$ , i.e.  $\Phi = \hat{\Phi}(\cdot, \cdot; \beta^c)$  can be treated in an analogous manner to that developed for single stage forming processes [33].

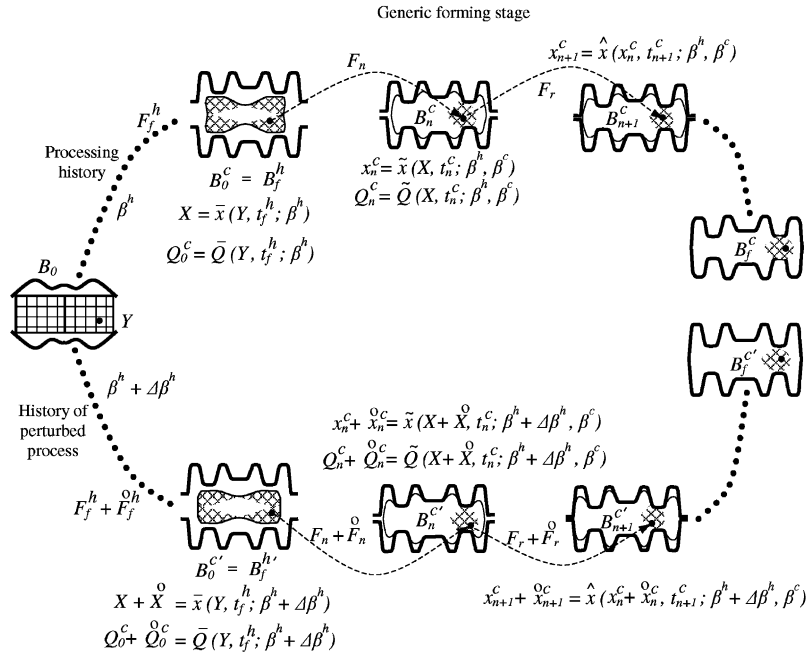


Fig 6. Schematic representation of the design sensitivity of the deformation in the current forming stage due to variations in the design parameters of previous forming stages.

To gain an insight on the definition and calculation of the sensitivities of Lagrangian fields in the current stage with respect to the history design variables  $\beta^h$ , we will take, for a moment, a total Lagrangian approach. In such an approach, the explicit dependence of Lagrangian fields on  $\beta^h$  i.e.  $\Phi = \hat{\Phi}(\cdot, \cdot; \beta^h)$  includes, (a) the variation of the current deformation as a result of changes in  $Q_0^c = \bar{Q}(X, t_0^c; \beta^h)$  which represents the collection of variables  $(F^p, s, \theta)$  in the intermediate preform  $\mathcal{B}_0^c$  and (b) the variation in the intermediate preform shape  $\mathcal{B}_0^c$  that results in between other in changes in the contact conditions during the current forming stage. These explicit dependencies are difficult to quantify directly. Lagrangian fields also depend implicitly on  $\beta^h$  through the variable  $X$  as a result of the deformation processing history.

For computing the sensitivity fields in the current stage with respect to the history design variables  $\beta^h$ , we consider Fig. 6. Consider the dependence of Lagrangian fields  $\Phi = \tilde{\Phi}(X, t)$  on  $\beta^h$ . This dependence can be expressed as follows

$$\Phi = \tilde{\Phi}(\bar{x}(Y, t_0^c; \beta^h), t; \beta^h) = \bar{\Phi}(Y, t; \beta^h), \quad t \in [t_0^c, t_f^c]. \tag{3.8}$$

The design differential  $\overset{\circ}{\Phi}$  of a Lagrangian field is defined as the total Gateaux differential of  $\Phi = \bar{\Phi}(Y, t; \beta^h)$  in the direction  $\Delta\beta^h$  computed at  $\beta^h$ :

$$\begin{aligned} \overset{\circ}{\Phi} &\equiv \tilde{\tilde{\Phi}}(X, t; \beta^h, \Delta\beta^h) = \bar{\bar{\Phi}}(Y, t; \beta^h, \Delta\beta^h) \\ &= \left. \frac{d}{d\omega} \bar{\Phi}(Y, t; \beta^h + \omega\Delta\beta^h) \right|_{\omega=0}, \quad t \in [t_0^c, t_f^c]. \end{aligned} \tag{3.9}$$

The design differential or sensitivity  $\overset{\circ}{\Phi}$  can be understood as representing the difference between two fields  $\bar{\Phi}$ , that result due to different designs defined by  $\beta^h$  and  $\beta^h + \Delta\beta^h$  (see Fig. 6), i.e.

$$\overset{\circ}{\Phi} = \bar{\Phi}(\mathbf{Y}, t; \beta^h + \Delta\beta^h) - \bar{\Phi}(\mathbf{Y}, t; \beta^h) + O(\|\Delta\beta^h\|^2), \quad t \in [t_0^c, t_f^c]. \quad (3.10)$$

It is emphasized that the fields  $\bar{\Phi}(\beta^h)$  and  $\bar{\Phi}(\beta^h + \Delta\beta^h)$  are computed for material points that occupy the same location  $\mathbf{Y}$  in the design independent virgin configuration  $\mathcal{B}_0$ . The design differentiation as shown in Eq. (3.9) is thus performed in the fixed virgin configuration  $\mathcal{B}_0$ . This configuration needs to be distinguished from the reference configuration  $\mathcal{B}_n^c$  that is used in the updated Lagrangian analysis.

Let us return to the dependence of  $\tilde{\Phi}(\mathbf{X}, t)$ ,  $t \in [t_0^c, t_f^c]$  on  $\beta^h$ . This dependence results from the fact that the intermediate preform shape  $\partial\mathcal{B}_0^c$  and key field variables distribution  $Q_0^c$  depend on  $\beta^h$ . In particular, one can write the following symbolic equations:

$$\tilde{\Phi}(\mathbf{X}, t; \beta^h) = \bar{\Phi}(\mathbf{Y}, t; \beta^h) = \bar{\Phi}(\mathbf{Y}, t; \partial\mathcal{B}_0^c(\beta^h), Q_0^c(\beta^h)), \quad t \in [t_0^c, t_f^c], \quad (3.11)$$

where  $\partial\mathcal{B}_0^c(\beta^h)$  and  $Q_0^c(\beta^h)$  are obtained for the given selection of  $\beta^h$ .

Using the definition of Eq. (3.9) and Eq. (3.11), one can obtain that

$$\overset{\circ}{\Phi} = \frac{\partial\bar{\Phi}(\mathbf{Y}, t; \partial\mathcal{B}_0^c, Q_0^c)}{\partial(\partial\mathcal{B}_0^c)} \left[ \frac{\partial(\partial\mathcal{B}_0^c)}{\partial\beta^h} [\Delta\beta^h] \right] + \frac{\partial\bar{\Phi}(\mathbf{Y}, t; \partial\mathcal{B}_0^c, Q_0^c)}{\partial Q_0^c} \left[ \frac{\partial Q_0^c}{\partial\beta^h} [\Delta\beta^h] \right], \quad t \in [t_0^c, t_f^c]. \quad (3.12)$$

To evaluate  $\overset{\circ}{\Phi}$ , one must thus first compute the Gateaux differentials of  $\partial\mathcal{B}_0^c$  and  $Q_0^c$  with respect to a perturbation  $\Delta\beta^h$  in the design parameters of all previous forming stages. These Gateaux differentials, which define perturbations in the intermediate preform shape and field variable set  $Q$  can be used to compute the Gateaux differential of  $\bar{\Phi}$  in the current forming stage. Thus, the computation of sensitivities for multi-stage processes must be performed in a sequential manner. The independent driving forces for the computation of sensitivities with respect to  $\beta^h$  in the current forming stage are the design differentials of  $\partial\mathcal{B}_0^c$  and  $Q_0^c$ . The recognition of the linear dependence of  $\overset{\circ}{\Phi}$  on these design differentials (Eq. (3.12)) enables the efficient computation of design sensitivities of the current forming stage as demonstrated in the developments that follow.

The dependence of an updated Lagrangian field  $\Phi = \hat{\Phi}(\mathbf{x}_n^c, t)$  on  $\beta^h$  can now be expressed as follows:

$$\Phi = \hat{\Phi}(\mathbf{x}_n^c, t; \beta^h) = \tilde{\Phi}(\mathbf{X}, t; \beta^h) = \bar{\Phi}(\mathbf{Y}, t; \beta^h), \quad t \in [t_0^c, t_f^c]. \quad (3.13)$$

The sensitivity  $\overset{\circ}{\hat{\Phi}} = \hat{\Phi}(\mathbf{x}_n^c, t; \beta^h, \Delta\beta^h)$  is then defined as the total Gateaux differential of  $\Phi = \hat{\Phi}(\mathbf{x}_n^c, t; \beta^h)$  in the direction  $\Delta\beta^h$  computed at  $\beta^h$

$$\begin{aligned} \overset{\circ}{\hat{\Phi}}(\mathbf{x}_n^c, t; \beta^h, \Delta\beta^h) &= \tilde{\tilde{\Phi}}(\mathbf{X}, t; \beta^h, \Delta\beta^h) = \bar{\bar{\Phi}}(\mathbf{Y}, t; \beta^h, \Delta\beta^h) \\ &= \frac{d}{d\lambda} \bar{\Phi}(\mathbf{Y}, t; \beta^h + \lambda\Delta\beta^h) \Big|_{\lambda=0}, \quad t \in [t_0^c, t_f^c]. \end{aligned} \quad (3.14)$$

The shape sensitivity  $\overset{\circ}{\Phi}$  represents the difference between two values of the field  $\Phi$ , that result due to two different initial configurations defined by the shape parameters  $\boldsymbol{\beta}^h + \Delta\boldsymbol{\beta}^h$  and  $\boldsymbol{\beta}^h$ , i.e.

$$\begin{aligned} \overset{\circ}{\Phi}(\mathbf{x}_n^c, t; \boldsymbol{\beta}^h, \Delta\boldsymbol{\beta}^h) &= \hat{\Phi}(\tilde{\mathbf{x}}(X, t_n^c; \boldsymbol{\beta}^h + \Delta\boldsymbol{\beta}^h), t; \boldsymbol{\beta}^h + \Delta\boldsymbol{\beta}^h) - \hat{\Phi}(\tilde{\mathbf{x}}(X, t_n^c; \boldsymbol{\beta}^h), t; \boldsymbol{\beta}^h) + O(\|\Delta\boldsymbol{\beta}^h\|^2) \\ &= \tilde{\Phi}(\tilde{\mathbf{x}}(Y; \boldsymbol{\beta}^h + \Delta\boldsymbol{\beta}^h), t; \boldsymbol{\beta}^h + \Delta\boldsymbol{\beta}^h) - \tilde{\Phi}(\tilde{\mathbf{x}}(Y; \boldsymbol{\beta}^h), t; \boldsymbol{\beta}^h) + O(\|\Delta\boldsymbol{\beta}^h\|^2) \\ &= \bar{\Phi}(Y, t; \boldsymbol{\beta}^h + \Delta\boldsymbol{\beta}^h) - \bar{\Phi}(Y, t; \boldsymbol{\beta}^h) + O(\|\Delta\boldsymbol{\beta}^h\|^2), \quad t \in [t_0^c, t_f^c]. \end{aligned} \tag{3.15}$$

Let us consider the dependence of  $\hat{\Phi}(\mathbf{x}_n^c, t_{n+1}^c)$  on  $\boldsymbol{\beta}^h$ . This dependence results in the solution of the incremental deformation problem in the current forming state from the fact that the reference shape  $\partial\mathcal{B}_n^c$  and field distribution  $Q_n^c$  depend on  $\boldsymbol{\beta}^h$ . In particular, one can write:

$$\hat{\Phi}(\mathbf{x}_n^c, t_{n+1}^c; \boldsymbol{\beta}^h) = \hat{\Phi}(\mathbf{x}_n^c, t_{n+1}^c; \partial\mathcal{B}_n^c(\boldsymbol{\beta}^h), Q_n^c(\boldsymbol{\beta}^h)). \tag{3.16}$$

Using the definition of Eq. (3.14) and Eq. (3.16), one can obtain that

$$\overset{\circ}{\Phi}(\mathbf{x}_n^c, t_{n+1}^c; \boldsymbol{\beta}^h) = \frac{\partial\hat{\Phi}(\mathbf{x}_n^c, t_{n+1}^c; \partial\mathcal{B}_n^c, Q_n^c)}{\partial(\partial\mathcal{B}_n^c)} \left[ \frac{\partial(\partial\mathcal{B}_n^c)}{\partial\boldsymbol{\beta}^h} [\Delta\boldsymbol{\beta}^h] \right] + \frac{\partial\hat{\Phi}(\mathbf{x}_n^c, t_{n+1}^c; \partial\mathcal{B}_n^c, Q_n^c)}{\partial Q_n^c} \left[ \frac{\partial Q_n^c}{\partial\boldsymbol{\beta}^h} [\Delta\boldsymbol{\beta}^h] \right]. \tag{3.17}$$

To evaluate  $\overset{\circ}{\Phi}$  in an updated Lagrangian framework, one must thus first compute the Gateaux differentials of  $\partial\mathcal{B}_{n+1}^c$  and  $Q_{n+1}^c$  with respect to  $\partial\mathcal{B}_n^c$  and  $Q_n^c$ , for  $n = 1, 2, \dots, f$ . In this incremental calculation, the effect of the previous processing history becomes apparent and relevant only as initial conditions at  $t = t_0^c$ :

$$\frac{\partial(\partial\mathcal{B}_0^c)}{\partial\boldsymbol{\beta}^h} [\Delta\boldsymbol{\beta}^h] = \frac{\partial(\partial\mathcal{B}_f^h)}{\partial\boldsymbol{\beta}^h} [\Delta\boldsymbol{\beta}^h], \tag{3.18}$$

$$\frac{\partial Q_0^c}{\partial\boldsymbol{\beta}^h} [\Delta\boldsymbol{\beta}^h] = \frac{\partial Q_f^h}{\partial\boldsymbol{\beta}^h} [\Delta\boldsymbol{\beta}^h]. \tag{3.19}$$

The calculations of Eq. (3.12), (3.18) and (3.19) indicate that the sequential updated Lagrangian approach proposed here treats various types of sensitivity fields in a unified manner, e.g. it allows Eqs. (3.17) to be used regardless if the initial conditions of Eqs. (3.18), (3.19) refer to shape or process-based sensitivities in the processing history.

In concluding this section, we note that unloading is combined with each forming stage, thus the sensitivity fields on the right hand side of Eqs. (3.18) and (3.19) are referred to the unloading stage after the last stage in the history of deformation processing.

#### 4. The continuum sensitivity method for a generic forming stage

The developed scheme adopts the ‘design-differentiate then discretize’ approach (see Fig. 7) instead of the ‘discretize then design-differentiate’ approach. The governing equations of the various

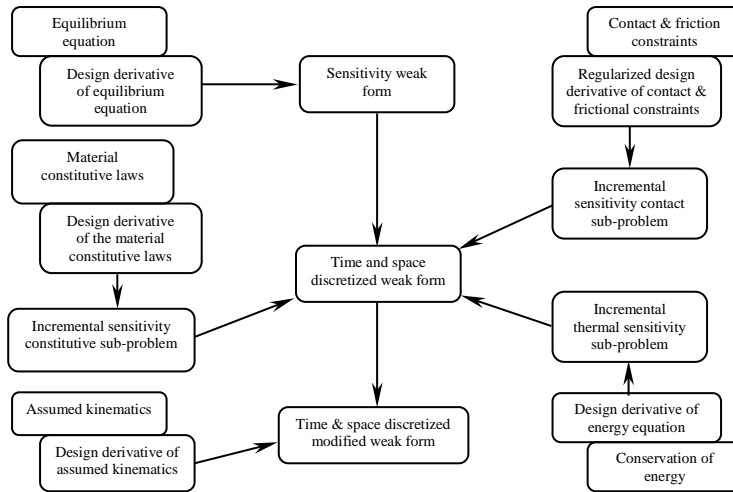


Fig 7. Schematic of the continuum sensitivity algorithm in a generic forming stage.

subproblems in the direct analysis (e.g. the kinematic, constitutive, contact and thermal analyses) are first design-differentiated and then appropriate weak forms, time integration and discretization are introduced. The resulting linear sensitivity subproblems can be coupled together in each forming stage to produce a linear problem for computing the sensitivity of the deformation, plastic deformation gradient and material state. A unified weak form is developed here to compute sensitivities with respect to any design parameter  $\beta$  in any stage. Appropriate features can then be identified which contrast the sensitivity analysis performed with respect to  $\beta^h$  from  $\beta^c$ . The sensitivity problem discussed here is posed using an updated Lagrangian formulation.

#### 4.1. Sensitivity kinematic problem in a generic forming stage

A weak form for the linear sensitivity analysis of a generic forming stage is identified by considering the sensitivity of the equilibrium equations and boundary conditions at the continuum level (Fig. 7). The sensitivity deformation problem is developed on the reference preform  $\mathcal{B}_n^c$ . The design sensitivity of the equilibrium equation (2.8) at  $t = t_{n+1}^c$  results in

$$\overline{\nabla_n \cdot \mathbf{P}_r} + \overset{\circ}{\mathbf{f}} = \mathbf{0}, \quad \forall \mathbf{x}_n^c \in \mathcal{B}_n^c. \tag{4.1}$$

A variational form for the above sensitivity equilibrium equation can finally be posed as follows [25]:

$$\begin{aligned} & \int_{\mathcal{B}_n^c} \overset{\circ}{\mathbf{P}}_r \cdot \nabla_n \tilde{\boldsymbol{\eta}} dV_n^c - \int_{\mathcal{B}_n^c} (\mathbf{P}_r [\nabla_n \cdot \mathbf{L}_n^{cT}]) \cdot \tilde{\boldsymbol{\eta}} dV_n^c - \int_{\mathcal{B}_n^c} (\mathbf{P}_r \mathbf{L}_n^{cT}) \cdot \nabla_n \tilde{\boldsymbol{\eta}} dV_n^c \\ & = \int_{\Gamma_n^c} \{ \overset{\circ}{\boldsymbol{\lambda}} - [\mathbf{L}_n^c \cdot (\mathbf{N} \otimes \mathbf{N})] \boldsymbol{\lambda} \} \cdot \tilde{\boldsymbol{\eta}} dA_n^c, \end{aligned} \tag{4.2}$$

where  $\tilde{\eta}$  is a kinematically admissible sensitivity deformation field expressed over the reference configuration  $\mathcal{B}_n^c$ ,  $\mathbf{N}$  is the unit normal vector to  $\Gamma_n^c$  and the (known) design velocity gradient  $\mathbf{L}_n^c$  at  $t_n^c$  is defined as follows:

$$\mathbf{L}_n^c \equiv \nabla_n \hat{\mathbf{x}}(\mathbf{x}_{n-1}^c, t_n^c; \boldsymbol{\beta}, \Delta\boldsymbol{\beta}) = \mathring{\mathbf{F}}_n^c \mathbf{F}_n^{c-1}. \tag{4.3}$$

It should be noted that the velocity design gradient  $\mathbf{L}_n^c$  is always computed with respect to the virgin configuration  $\mathcal{B}_0$ . In the time incremental sensitivity computations, the velocity gradient at the beginning of the current forming process at  $t = t_0^c$  is specified through the initial conditions given in Eqs. (3.18), (3.19). The primary unknown of Eq. (4.2) is the design differential  $\hat{\mathbf{x}}_{n+1}^c = \hat{\mathbf{x}}(\mathbf{x}_n^c, t_{n+1}^c; \boldsymbol{\beta}, \Delta\boldsymbol{\beta})$ . In order to obtain the final form of the variational sensitivity problem, the relationships between (a)  $\mathring{\mathbf{F}}_r$  and  $\hat{\mathbf{x}}_{n+1}^c$  (b)  $\mathring{\mathbf{P}}_r$  and  $[\hat{\mathbf{x}}_{n+1}^c, \hat{\theta}_{n+1}^c]$  (c)  $\mathring{\boldsymbol{\lambda}}$  and  $\hat{\mathbf{x}}_{n+1}^c$  need to be developed. The relationship between  $\mathring{\mathbf{F}}_r$  and  $\hat{\mathbf{x}}_{n+1}^c$  is purely kinematic and is given as follows:

$$\mathring{\mathbf{F}}_r = \overline{\nabla_n \hat{\mathbf{x}}_{n+1}^c} = \nabla_n \hat{\mathbf{x}}_{n+1}^c - \mathbf{F}_r \mathbf{L}_n^c. \tag{4.4}$$

The relationship between  $\mathring{\mathbf{P}}_r$  and  $[\hat{\mathbf{x}}_{n+1}^c, \hat{\theta}_{n+1}^c]$  is obtained from the sensitivity constitutive problem and takes the form:

$$\mathring{\mathbf{P}}_r = \mathcal{A}[\mathring{\mathbf{F}}_r] + B \hat{\theta}_{n+1}^c + C, \tag{4.5}$$

where  $\mathcal{A}$  is a fourth order tensor and  $B, C$  are second order tensors. These tensors are constants defined from known direct fields at the current time step and sensitivity fields at the previous time step (see Section 4.2). The relationship between  $\mathring{\boldsymbol{\lambda}}$  and  $\hat{\mathbf{x}}_{n+1}^c$  is obtained from the sensitivity contact problem as (see Section 4.4):

$$\mathring{\boldsymbol{\lambda}} = D[\hat{\mathbf{x}}_{n+1}^c] + d, \tag{4.6}$$

where  $D$  is a second order tensor and  $d$  a vector. The derivation of these tensors resulting by design-differentiation of a regularized contact problem can be found in [26].

Consistent with the direct deformation analysis where an assumed (discrete) representation of the deformation gradient  $\mathbf{F}_r$  was used in the FE solution of the weak form, a sensitivity analysis is developed for the FE solution of the assumed strain  $\mathbf{F}$ -bar method. Let us denote the terms in the left-hand side of the sensitivity weak form in eq. (4.2) by  $\mathcal{S}^{int}$ . The assumed strain sensitivity analysis involves the modification of the term  $\mathcal{S}^{int}$  in the FE representation of the sensitivity weak form. In the  $\mathbf{F}$ -bar method, only the constitutive response is modified. Thus  $\mathring{\mathbf{P}}_r \equiv \mathring{\mathbf{P}}_r(\mathring{\mathbf{F}}_h^{ave}, \hat{\theta}_{n+1}^c)$  takes the form

$$\mathring{\mathbf{P}}_r = \mathcal{A}[\mathring{\mathbf{F}}_h^{ave}] + B \hat{\theta}_{n+1}^c + C. \tag{4.7}$$

The assumed (discrete) sensitivity deformation gradient is obtained by the design differentiation of the volumetric-deviatoric decomposition introduced in eq. (2.20) (Fig. 4):

$$\mathring{\mathbf{F}}_h^{ave} = \varepsilon \mathring{\mathbf{F}}_h + (1 - \varepsilon) \bar{\mathring{\mathbf{F}}}_h,$$

$$\begin{aligned}\overset{\circ}{\mathbf{F}}_h &= \overset{\circ}{\mathbf{F}}_h^{vol} \mathbf{F}_h^{dev} + \bar{\mathbf{F}}_h^{vol} \overset{\circ}{\mathbf{F}}_h^{dev}, \\ \overset{\circ}{\mathbf{F}}_h^{vol} &= \frac{1}{3} \bar{J}_h^{-2/3} \left[ \sum_{a=1}^{NINT} J_{ha}(\bar{\xi}_a) \text{tr}[\overset{\circ}{\mathbf{F}}_h(\bar{\xi}_a) \mathbf{F}_h^{-1}(\bar{\xi}_a)] \bar{N}_a \right] \mathbf{I}, \\ \overset{\circ}{\mathbf{F}}_h^{dev} &= J_h^{-1/3} \overset{\circ}{\mathbf{F}}_h - \frac{1}{3} J_h^{-1/3} \mathbf{F}_h \text{tr}[\overset{\circ}{\mathbf{F}}_h \mathbf{F}_h^{-1}].\end{aligned}\quad (4.8)$$

Using the expressions given above, the assumed sensitivity deformation gradient which is used in the FE representation of the sensitivity weak form is given as follows:

$$\begin{aligned}\overset{\circ}{\mathbf{F}}_h^{ave} &= \left\{ \varepsilon \overset{\circ}{\mathbf{F}}_h + (1 - \varepsilon) \left[ \frac{\bar{J}_h}{J} \right]^{1/3} \overset{\circ}{\mathbf{F}}_h \right\} + \frac{1 - \varepsilon}{3} \left[ \sum_{a=1}^{NINT} J_{ha}(\bar{\xi}_a) \text{tr}[\overset{\circ}{\mathbf{F}}_h(\bar{\xi}_a) \mathbf{F}_h^{-1}(\bar{\xi}_a)] \bar{N}_a \right] \bar{J}_h^{-1} \bar{\mathbf{F}}_h \\ &\quad - \frac{1 - \varepsilon}{3} \{ \text{tr}[\overset{\circ}{\mathbf{F}}_h \mathbf{F}_h^{-1}] \bar{\mathbf{F}}_h \}.\end{aligned}$$

The term in the first parenthesis has the identical form that relates  $\mathbf{F}_h^{ave}$  and  $\mathbf{F}_h$  in the direct deformation problem. The latter terms result due to the fact that the assumed material gradient relationship depends on the current state of deformation and needs to be linearized as well. To complete the analysis, the kinematic relationship between  $\overset{\circ}{\mathbf{F}}_h^{ave}$  and  $\overset{\circ}{\mathbf{x}}_{n+1}^c$  needs to be developed. This is obtained by using Eq. (4.4) in the expressions for  $\overset{\circ}{\mathbf{F}}_h$  and  $\overset{\circ}{\mathbf{F}}_h(\bar{\xi}_a)$ :

$$\begin{aligned}\overset{\circ}{\mathbf{F}}_h &= \nabla_n \overset{\circ}{\mathbf{x}}_{n+1}^c - \mathbf{F}_h \mathbf{L}_n^c, \\ \overset{\circ}{\mathbf{F}}_h(\bar{\xi}_a) &= \nabla_n \overset{\circ}{\mathbf{x}}_{n+1}^c(\bar{\xi}_a) - \mathbf{F}_h(\bar{\xi}_a) \mathbf{L}_n^c(\bar{\xi}_a).\end{aligned}\quad (4.9)$$

The modified term  $\mathcal{S}^{int}$  in the finite element representation is given as follows:

$$\mathcal{S}_h^{int} \equiv \sum_e \int_{\Omega_e} \{ \overset{\circ}{\mathbf{P}}_r(\overset{\circ}{\mathbf{F}}_h^{ave}) - [\mathbf{P}_r(\mathbf{F}_h^{ave}) \mathbf{L}_n^{cT}] \} \cdot \nabla_n \tilde{\mathbf{q}}_h \, dV_n^c - \int_{\Omega_e} (\mathbf{P}_r(\mathbf{F}_h^{ave}) [\nabla_n \cdot \mathbf{L}_n^{cT}]) \cdot \tilde{\mathbf{q}}_h \, dV_n^c.$$

#### 4.2. Sensitivity constitutive problem in a generic forming stage

In the following analysis, we drop the superscript  $c$  in most of the symbols but we emphasize that all equations here are referred to the generic current forming stage. As part of this sub-problem, the relationship between  $\overset{\circ}{\mathbf{P}}_r$  and  $[\overset{\circ}{\mathbf{F}}_r, \overset{\circ}{\theta}_{n+1}^c]$  at time  $t_{n+1}^c$  as used in the solution of the sensitivity deformation problem is computed. The solution of the direct deformation problem is known at time  $t_{n+1}^c$ . Due to the non linear material response, the constitutive sensitivity problem is history dependent and the solution  $[\overset{\circ}{\mathbf{T}}, \overset{\circ}{s}, \overset{\circ}{\mathbf{F}}^e, \overset{\circ}{\theta}]$  of the sensitivity problem at time  $t_n^c$  is known. Thus, the solution of the sensitivity constitutive sub-problem needs to be advanced within the incremental solution scheme by integrating the evolution equations for the sensitivity of the plastic deformation gradient  $\mathbf{F}^p$ , the evolution equation for the sensitivity of the state variable  $s$  and the evolution equation for the sensitivity of the temperature  $\theta$ .

As part of the update procedure, one computes the set  $[\overset{\circ}{\mathbf{T}}, \overset{\circ}{s}, \overset{\circ}{\mathbf{F}}^e, \overset{\circ}{\theta}]$  at the end of the time increment  $t_{n+1}^c$  where the sensitivity of the total deformation gradient  $\overset{\circ}{\mathbf{F}}_{n+1}^c$  and the sensitivity of the temperature field  $\overset{\circ}{\theta}_{n+1}^c$  are assumed known.

The evolution of the sensitivity of the plastic deformation gradient  $\mathbf{F}^p$  is obtained by the design differentiation of the flow rule as

$$\frac{\partial \overset{\circ}{\mathbf{F}}^p}{\partial t} = \bar{\mathbf{D}}^p \overset{\circ}{\mathbf{F}}^p + \overset{\circ}{\mathbf{D}}^p \mathbf{F}^p. \tag{4.10}$$

Taking the design-derivative (sensitivity) of the flow rule (Eq. (2.11)) and by design differentiation of the hyperelastic law one can show that  $\overset{\circ}{\mathbf{D}}^p$  depends explicitly only on  $\overset{\circ}{\mathbf{F}}^e$  and not on  $\overset{\circ}{\mathbf{F}}^p$ .

The evolution equation for  $\overset{\circ}{s}$  is obtained by taking the direct variation of the state variable evolution (Eq. (2.13)):

$$\frac{\partial \overset{\circ}{s}}{\partial t} = g_{\bar{\sigma}} \overset{\circ}{\bar{\sigma}} + g_s \overset{\circ}{s} + g_{\theta} \overset{\circ}{\theta}. \tag{4.11}$$

The evolution equation for  $\overset{\circ}{\mathbf{F}}^{\theta}$  can be derived by considering the direct variation of Eq. (2.4). With time integration of the resulting equation, one can easily show that

$$\overset{\circ}{\mathbf{F}}_{n+1}^{\theta} = \beta \overset{\circ}{\theta}_{n+1}^c \mathbf{F}_{n+1}^{\theta}. \tag{4.12}$$

An Euler-backward integration scheme over  $(t_n^c, t_{n+1}^c)$  applied to the evolution equations for the sensitivities of the plastic deformation gradient (Eq. (4.10)), scalar state variable (Eq. (4.11)) and thermal deformation gradient (Eq. (4.12)) yields [35]:

- Sensitivity of the plastic deformation gradient at time  $t_{n+1}^c$ :

$$\overset{\circ}{\mathbf{F}}_{n+1}^p (\mathbf{F}_{n+1}^p)^{-1} = \Delta \mathbf{F}^p \overset{\circ}{\mathbf{F}}_{n+1}^p (\mathbf{F}_n^p)^{-1} (\Delta \mathbf{F}^p)^{-1} + \Delta t \overset{\circ}{\mathbf{D}}_{n+1}^p, \tag{4.13}$$

where from the constitutive subproblem of the direct problem [29],

$$\Delta \mathbf{F}^p = \mathbf{F}_{n+1}^p (\mathbf{F}_n^p)^{-1} = \exp(\Delta t \bar{\mathbf{D}}_{n+1}^p) \tag{4.14}$$

with  $\Delta t = t_{n+1}^c - t_n^c$ .

- Sensitivity of the scalar state variable at time  $t_{n+1}^c$ :

$$\overset{\circ}{s}_{n+1} = \frac{\overset{\circ}{s}_n + (g_{\bar{\sigma}})_{n+1} \Delta t \overset{\circ}{\bar{\sigma}}_{n+1} + (g_{\theta})_{n+1} \Delta t \overset{\circ}{\theta}_{n+1}^c}{1 - \Delta t (g_s)_{n+1}}. \tag{4.15}$$

It is noted that the deformation gradients  $\mathbf{F}_{n+1}^e$ ,  $\mathbf{F}_{n+1}^p$  and  $\mathbf{F}_{n+1}^{\theta}$  used here are the corresponding field values at  $t = t_{n+1}^c$  of the gradients  $\mathbf{F}^e$ ,  $\mathbf{F}^p$  and  $\mathbf{F}^{\theta}$  introduced in Eq. (2.3) using the multiplicative decomposition of the total deformation gradient  $\mathbf{F}_{n+1}^c$ . Substituting the linear relation between  $\overset{\circ}{\mathbf{D}}^p$  and  $\overset{\circ}{\mathbf{F}}^e$  and Eq. (4.15) in Eq. (4.13), one can finally derive the linear relation between  $\overset{\circ}{\mathbf{F}}_{n+1}^p$  and  $[\overset{\circ}{\mathbf{F}}_{n+1}^e, \overset{\circ}{\theta}_{n+1}^c]$ .

For deriving the linear relation between  $\overset{\circ}{\mathbf{F}}_{n+1}^e$  and  $[\overset{\circ}{\mathbf{F}}_{n+1}^c, \overset{\circ}{\theta}_{n+1}^c]$ , one can start by taking the sensitivity of the multiplicative decomposition of the deformation gradient (Eq. (2.3)). After some algebraic manipulations, one can write the following:

$$(\mathbf{F}_{n+1}^e)^{-1} \overset{\circ}{\mathbf{F}}_{n+1}^c (\mathbf{F}_{n+1}^c)^{-1} \mathbf{F}_{n+1}^e = (\mathbf{F}_{n+1}^e)^{-1} \overset{\circ}{\mathbf{F}}_{n+1}^e + \overset{\circ}{\mathbf{F}}_{n+1}^p (\mathbf{F}_{n+1}^p)^{-1} + \beta \overset{\circ}{\theta}_{n+1}^c \mathbf{I}. \quad (4.16)$$

Substitution of the earlier obtained linear relation between  $\overset{\circ}{\mathbf{F}}_{n+1}^p$  and  $[\overset{\circ}{\mathbf{F}}_{n+1}^e, \overset{\circ}{\theta}_{n+1}^c]$  in Eq. (4.16) results in a linear relation between  $\overset{\circ}{\mathbf{F}}_{n+1}^e$  and  $[\overset{\circ}{\mathbf{F}}_{n+1}^c, \overset{\circ}{\theta}_{n+1}^c]$ . Using the sensitivity of Eq. (2.2), one can easily derive the linear relation between  $\overset{\circ}{\mathbf{F}}_{n+1}^c$  and  $\overset{\circ}{\mathbf{F}}_r$  and thus the linear relation between  $\overset{\circ}{\mathbf{F}}_{n+1}^e$  and  $\overset{\circ}{\mathbf{F}}_r$ . Similarly, one can transform the linear relation of the sensitivity of any field with  $\overset{\circ}{\mathbf{F}}_{n+1}^c$  to a linear relation of the sensitivity of the field with  $\overset{\circ}{\mathbf{F}}_r$ .

In computing the sensitivity of the temperature field in the workpiece (see Section 4.3), one needs to evaluate the sensitivity  $\overset{\circ}{\mathcal{W}}_{mech}$  of the mechanical dissipation  $\mathcal{W}_{mech}$ . Using Eq. (2.12), one can compute  $\overset{\circ}{\mathcal{W}}_{mech}$  as follows:

$$\begin{aligned} \overset{\circ}{\mathcal{W}}_{mech} &= \omega(\overset{\circ}{\tilde{\sigma}} f + \tilde{\sigma} \overset{\circ}{f}) \\ &= \omega[(f + \tilde{\sigma} f_{\tilde{\sigma}}) \overset{\circ}{\tilde{\sigma}} + \tilde{\sigma} f_s \overset{\circ}{s} + \tilde{\sigma} f_{\theta} \overset{\circ}{\theta}], \end{aligned} \quad (4.17)$$

where in this work, the fraction  $\omega$  of the plastic work that contributes to the mechanical dissipation is taken as  $\omega = 0.9$ . Using the sensitivity of the hyperelastic law, one can derive a linear relation between  $\overset{\circ}{\mathcal{W}}_{mech}$  and  $[\overset{\circ}{\mathbf{F}}_{n+1}^e, \overset{\circ}{\theta}_{n+1}^c]$  at  $t_{n+1}^c$ .

The sensitivity constitutive sub-problem is essentially identical for studying variations with respect to  $\beta^h$  or  $\beta^c$ . The sensitivity deformation problem presented here can also be used in the analysis of the sensitivity of the unloading process at the end of each forming stage. In this case, we need to consider the sensitivity of a finite deformation elasto-static problem. Thus the sensitivity constitutive problem presented above is modified and the material deformation behavior treated as elastic in the unloading phase. In particular, the relationship between  $\overset{\circ}{\mathbf{P}}_r$  and  $[\overset{\circ}{\mathbf{F}}_r, \overset{\circ}{\theta}_{n+1}^c]$  is determined by an elastic constitutive law, i.e.  $\overset{\circ}{\mathbf{F}}_u^p = \overset{\circ}{\mathbf{F}}^p$ . The duration in between forming stages is characterized by the evolution of the sensitivity of the inelastic internal variable (recovery phase).

#### 4.3. Sensitivity thermal problem

Consider the sensitivity thermal evolution equation at  $t = t_{n+1}^c$  obtained by the design differentiation of the classical energy equation in the workpiece [35]:

$$\rho c \frac{\partial \overset{\circ}{\theta}}{\partial t} + (\rho c)' \overset{\circ}{\theta} \frac{\partial \overset{\circ}{\theta}}{\partial t} = \overset{\circ}{\mathcal{W}}_{mech} - \overset{\circ}{\nabla}_{n+1} \cdot \mathbf{q}, \quad (4.18)$$

where here ( $'$ ) denotes derivative of a scalar function with respect to its argument. Using Fourier's first law, the sensitivity of the spatial divergence of the heat flux can finally be expressed as

follows:

$$\begin{aligned} \overline{\nabla_{n+1} \cdot \mathbf{q}} = & -\nabla_Y(K\nabla_{n+1}\overset{\circ}{\theta}_{n+1}^c) \cdot (\mathbf{F}_{n+1}^c)^{-T} - \nabla_Y((\mathbf{L}_{n+1}^c)^T \mathbf{q}) \cdot (\mathbf{F}_{n+1}^c)^{-T} \\ & - \nabla_Y \mathbf{q} \cdot (\mathbf{L}_{n+1}^c)^T (\mathbf{F}_{n+1}^c)^{-T} - \nabla_Y(K' \overset{\circ}{\theta}_{n+1}^c \nabla_{n+1} \theta_{n+1}^c) \cdot (\mathbf{F}_{n+1}^c)^{-T} \end{aligned} \quad (4.19)$$

where  $\nabla_Y$  refers to the gradient with respect to the fixed virgin configuration  $\mathcal{B}_0$ . The above equation is then substituted in Eq. (4.18) and an Euler-backward time integration is performed. It is straightforward to then derive the following weak form of the thermal sensitivity equations [35]: For every admissible  $\vartheta$ ,

$$\begin{aligned} & \int_{\mathcal{B}_{n+1}^c} \frac{\rho c}{\Delta t} (\overset{\circ}{\theta}_{n+1}^c - \overset{\circ}{\theta}_n^c) \vartheta \, dV_{n+1}^c + \int_{\mathcal{B}_{n+1}^c} \frac{(\rho c)'}{\Delta t} (\theta_{n+1}^c - \theta_n^c) \overset{\circ}{\theta}_{n+1}^c \vartheta \, dV_{n+1}^c \\ & + \int_{\mathcal{B}_{n+1}^c} K \nabla_{n+1} \overset{\circ}{\theta}_{n+1}^c \cdot \nabla_{n+1} \vartheta \, dV_{n+1}^c + \int_{\mathcal{B}_{n+1}^c} K' \overset{\circ}{\theta}_{n+1}^c \nabla_{n+1} \theta_{n+1}^c \cdot \nabla_{n+1} \vartheta \, dV_{n+1}^c \\ & + \int_{\partial \mathcal{B}_{n+1}^c} [\overset{\circ}{\mathbf{q}}_{n+1}] \cdot \mathbf{n} \vartheta \, dA_{n+1} = \int_{\mathcal{B}_{n+1}^c} \overset{\circ}{\mathcal{W}}_{mech,n+1} \vartheta \, dV_{n+1}^c \\ & + \int_{\mathcal{B}_{n+1}^c} \nabla_{n+1} \mathbf{q}_{n+1} \cdot \mathbf{L}_{n+1}^c \vartheta \, dV_{n+1}^c - \int_{\mathcal{B}_{n+1}^c} (\mathbf{L}_{n+1}^c)^T \mathbf{q}_{n+1} \cdot \nabla_{n+1} \vartheta \, dV_{n+1}^c \end{aligned} \quad (4.20)$$

The primary unknowns of Eq. (4.20) are the design differentials  $\overset{\circ}{\mathbf{x}}_{n+1}^c = \overline{\mathbf{X}}(\mathbf{Y}, t_{n+1}^c; \boldsymbol{\beta}, \Delta \boldsymbol{\beta})$  and  $\overset{\circ}{\theta}_{n+1}^c = \overline{\theta}(\mathbf{Y}, t_{n+1}^c; \boldsymbol{\beta}, \Delta \boldsymbol{\beta})$ . In order to obtain the final form of the variational sensitivity problem, the relationships between (a)  $\overset{\circ}{\mathbf{F}}_r$  and  $\overset{\circ}{\mathbf{x}}_{n+1}^c$  (b)  $\overset{\circ}{\mathcal{W}}_{mech,n+1}$  and  $[\overset{\circ}{\mathbf{x}}_{n+1}^c, \overset{\circ}{\theta}_{n+1}^c]$  are needed. The derivation of these relationships was highlighted earlier.

The sensitivity thermal boundary conditions considered here are of the form

$$\overset{\circ}{\mathbf{q}} \cdot \mathbf{n} = -\mathbf{q} \cdot \overset{\circ}{\mathbf{n}} \quad \text{Neumann b.c.}, \quad (4.21)$$

$$\overset{\circ}{\mathbf{q}} \cdot \mathbf{n} = -\mathbf{q} \cdot \overset{\circ}{\mathbf{n}} + h_0 \overset{\circ}{\theta}_{n+1}^c \quad \text{Convective b.c.}, \quad (4.22)$$

$$\overset{\circ}{\mathbf{q}} \cdot \mathbf{n} = -\mathbf{q} \cdot \overset{\circ}{\mathbf{n}} + h_c (\overset{\circ}{\theta}_{n+1}^c - \overset{\circ}{\theta}_d) \quad \text{Contact b.c.}, \quad (4.23)$$

where  $h_0, h_c$  are the heat transfer coefficients in the free and contact surfaces of the workpiece, respectively and  $\overset{\circ}{\theta}_d$  refers to the sensitivity of the die temperature. Thermo-mechanical contact is not considered in this work and the dies are considered to be isothermal ( $\overset{\circ}{\theta}_d = 0$ ).

#### 4.4. Sensitivity contact problem in a generic forming stage

As part of this sub-problem, the relationship between the sensitivity of the contact traction  $\overset{\circ}{\boldsymbol{\lambda}}$  and  $\overset{\circ}{\mathbf{x}}_{n+1}^c$  at time  $t_{n+1}^c$  as used in the solution of the sensitivity deformation problem is computed. The sensitivity of a function  $f = f(\mathbf{x})$ , denoted by  $\overline{f(\mathbf{x})}$  generally consists of two parts, the first part,

$\overset{\circ}{f}$ , denotes the contribution due to changes in the function  $f$  with  $\mathbf{x}$  constant and the second part,  $\nabla f \overset{\circ}{\mathbf{x}}$ , denotes the contribution due to changes in the variable  $\mathbf{x}$  with  $f$  constant:

$$\overline{\overset{\circ}{f(\mathbf{x})}} = \overset{\circ}{f} + \nabla f \overset{\circ}{\mathbf{x}}. \tag{4.24}$$

In the case where the design parameter  $\beta$  represents the die shape, explicit changes in the die shape are represented by  $\overset{\circ}{\mathbf{y}}_{\beta}(\xi) = \mathbf{y}_{(\beta+\Delta\beta)}(\xi) - \mathbf{y}_{\beta}(\xi)$  and result in explicit changes in the normal and tangential vectors to the die ( $\overset{\circ}{\mathbf{v}}_{\beta}, \overset{\circ}{\mathbf{r}}_{\beta}$ ). For computing the sensitivity with respect to all other parameters  $\beta$ , one can write  $\overset{\circ}{\mathbf{y}}_{\beta} = \mathbf{0}$ .

As a result of the non-smooth nature of the contact/friction conditions and to allow for differentiability, the following regularizing assumptions are made in the computation of the sensitivities: *Transition from stick to slip condition and/or from contact to non-contact (or vice versa) does not occur at a material point as a result of a perturbation to the design parameters [25].*

Consideration of the strong form of the normal contact constraints (Eq. (2.16)) in the direct deformation problem yields for points in contact  $\mathcal{G}(\mathbf{x}_{n+1}^c) = 0$  and  $\lambda_N > 0$ . Thus, the normal contact sensitivity constraint is obtained as  $\overline{\overset{\circ}{\mathcal{G}(\mathbf{x}_{n+1}^c)}} = 0$  and  $\overset{\circ}{\lambda}_N \in \mathfrak{R}$ . The following penalty form is used to enforce this constraint:

$$\overset{\circ}{\lambda}_N = \overset{\circ}{\lambda}_{N_n^c} + \varepsilon_N \overline{\overset{\circ}{\mathcal{G}(\mathbf{x}_{n+1}^c)}}, \tag{4.25}$$

where  $\overset{\circ}{\lambda}_{N_n^c}$  is the sensitivity of the normal traction component at the beginning of the time integration step and  $\varepsilon_N$  the normal penalty parameter. Consideration of the tangential contact constraints yields that for points in sticking contact,  $\overset{\circ}{\xi} = 0$ . The corresponding sensitivity constraint takes the form: penalty formulation of the sticking sensitivity constraint is introduced:

$$\overset{\circ}{\xi} = \frac{1}{\varepsilon_T} \overset{\circ}{\lambda}_T, \tag{4.26}$$

where  $\varepsilon_T$  is the tangential penalty parameter. Integration of this equation results in the following:

$$\overset{\circ}{\lambda}_T = \overset{\circ}{\lambda}_{T_n^c} + \varepsilon_T (\overset{\circ}{\xi} - \overset{\circ}{\xi}_n^c), \tag{4.27}$$

where  $\overset{\circ}{\lambda}_{T_n^c}$  is the sensitivity of the tangential traction component at the beginning of the time integration step. In the case of slip,  $\overset{\circ}{\lambda}_T$  is well defined by the Coulomb friction law as

$$\overset{\circ}{\lambda}_T = \overline{\left( \mu \lambda_N \frac{1}{\|\boldsymbol{\tau}_1\|} \right)}. \tag{4.28}$$

The sensitivity of the contact traction vector is given as

$$\overset{\circ}{\boldsymbol{\lambda}} = \overline{\overset{\circ}{\lambda}_N \mathbf{v}(\bar{\mathbf{y}})} - \overline{\overset{\circ}{\lambda}_T \boldsymbol{\tau}_1(\bar{\mathbf{y}})} \tag{4.29}$$

and can be shown to take the following form [25,26]:

$$\overset{\circ}{\boldsymbol{\lambda}} = \overset{\circ}{\mathcal{G}} \boldsymbol{\gamma}_1 + \overset{\circ}{\xi} \boldsymbol{\gamma}_2 + \boldsymbol{\gamma}_3, \tag{4.30}$$

where  $\gamma_i$  are known vectors computed using the developments described above. It can be shown that,  $\overset{\circ}{\zeta}$  which represents the sensitivity of the amount of inelastic slip is related to  $\overset{\circ}{\mathbf{x}}_{n+1}^c$ . This linear relationship between  $\overset{\circ}{\zeta}$  and  $\overset{\circ}{\mathbf{x}}_{n+1}^c$  can be developed by consideration of the fact that the closest point  $\bar{\mathbf{y}}$  on the die to a point  $\mathbf{x}_{n+1}^c$  is the projection of the point  $\mathbf{x}_{n+1}^c$  on to the die. The linear relationship between the sensitivity of the gap function  $\overline{\mathcal{G}(\mathbf{x}_{n+1}^c)}$  and  $\overset{\circ}{\mathbf{x}}_{n+1}^c$  can be obtained by the design differentiation of the gap function [25].

### 5. Design examples

Design forming problems will herein be posed as optimization problems. Let the objective function be defined in terms of a Lagrangian field  $\mathbf{Z}(\mathbf{X}, t; \boldsymbol{\beta})$ , where herein the design vector  $\boldsymbol{\beta}$  is represented as a set of scalar variables  $\beta_1, \beta_2, \dots, \beta_M$ . The gradient of the objective function with respect to the design variables  $\beta_i$  will be calculated using the developed continuum sensitivity method. Let us suppose that the sensitivity problem has been solved for a particular choice of infinitesimally small and a priori specified  $\Delta\beta_i, i = 1, 2, \dots, M$ . We can then write the following:

$$\overset{\circ}{\mathbf{Z}}(\mathbf{X}, t; \beta_1, \beta_2, \dots, \beta_M, \Delta\beta_1, \Delta\beta_2, \dots, \Delta\beta_M) = \sum_{i=1}^M \frac{\partial \mathbf{Z}}{\partial \beta_i} \Delta\beta_i. \tag{5.1}$$

Therefore,

$$\frac{\partial \mathbf{Z}}{\partial \beta_i} = \frac{\overset{\circ}{\mathbf{Z}}(\mathbf{X}, t; \beta_1, \beta_2, \dots, \beta_M, 0, 0, \dots, \Delta\beta_i, \dots, 0)}{\Delta\beta_i}. \tag{5.2}$$

The computation of the gradient,  $\nabla \mathbf{Z}$  at each stage of the optimization process will thus require the solution of  $M$  CSM-based linear sensitivity problems in addition to the solution of the non-linear direct problem.

Three axisymmetric two-stage forming design examples are presented here with various objective functions defined at the product obtained at the end of the second stage. In all examples considered, the initial workpiece  $\mathcal{B}_0$  is of a given fixed volume. The total stroke during any stage is variable. The total height reduction at  $r = 0$ , i.e., along the  $z$ -axis, in any stage, is fixed. This fixed reduction, along with the profile of the die and workpiece fix the total stroke. The material chosen for the workpiece is 1100-Al at a temperature of 673 K. The isotropic state variable sinh-model of Brown et al. is used in this work. The pertinent functional forms and parameters for Eqs. (2.7), (2.12) and (2.13) are given in Refs. [35,36]. The thermal properties,  $\beta, K$  and  $\rho c$  introduced in Sections 2, 4.2 and 4.3 are here taken for 1100-Al to be  $26.5 \times 10^{-6} \text{ K}^{-1}$ ,  $238.0 \text{ N}/(\text{sec-K})$  and  $2.820 \text{ MN}/(\text{m}^2\text{-K})$ , respectively [35].

The F-bar method with a stabilization factor  $\varepsilon = 10^{-03}$  and four noded quadrilateral elements is used in the simulation.

The die is repositioned in the beginning of the second stage so that there is always exactly one simulation step  $V\Delta t$  between the die and the workpiece, where  $V$  is the die speed here taken as 0.01 mm/secs for both stages. This one step is used in our design simulator to model an unloading process until the workpiece touches the die and the second forming stage proceeds. During the

unloading process (i.e. after the removal of the first die), we assume for simplicity that the workpiece is gripped by its circumference and that the grip does not impose any stresses on the workpiece. Immediately after this unloading step, we make sure that the die comes in contact with the workpiece. This ensures that the problem under consideration can be still modelled as an axisymmetric problem. We thus assume that in all examples the exchange of the two dies occurs within one simulation step. Additional required time for this exchange will affect the temperature distribution within the workpiece and thus the state variable distribution (even though, we herein assume that the static recovery function  $\dot{r} = 0$  (Eq. (2.13))).

### 5.1. Preforming die design in open-die hot forging to minimize barreling (Example 1)

Let us consider an initial workpiece in the form of a right circular cylinder of radius  $r = 1.0$  mm and height 2.0 mm. The objective in this example is to design the die shape in the preforming stage, so that the product after the finishing stage is a right circular cylinder of radius  $r_0 = 1.414$  mm and height 1.0 mm, i.e. a final product of a given height with no barreling. The height reduction at  $r = 0$ , in the first stage is 0.6 mm and in the second stage is 0.4 mm. The friction coefficient for both stages is taken as 0.2, the initial workpiece temperature is set at 673 K and the heat transfer coefficients are taken as  $h_0 = h_c = 6.7$  W/m<sup>2</sup> K.

The die contact surface is represented using a degree 6 Bézier curve with 5 independent variables.

$$r(\alpha) = 1.5\alpha, \quad z_\beta(\alpha) = \sum_{i=1}^7 \beta_i \phi_i(\alpha). \quad (5.3)$$

The die height at  $r = 0$  was specified and the die shape is assumed to have a zero slope at  $r = 0$ . The following basis functions:

$$\begin{aligned} \phi_1 &= (1 - \alpha)^6, & \phi_2 &= 6(1 - \alpha)^5\alpha, & \phi_3 &= 15(1 - \alpha)^4\alpha^2, & \phi_4 &= 20(1 - \alpha)^3\alpha^3, \\ \phi_5 &= 15(1 - \alpha)^2\alpha^4, & \phi_6 &= 6(1 - \alpha)\alpha^5, & \phi_7 &= \alpha^7. \end{aligned} \quad (5.4)$$

are assumed. We herein choose  $\beta_6$  and  $\beta_7 = 1.3$  mm, in order to fix the height and slope at  $r = 0$ .

The finite dimensional optimization problem is posed as follows:

$$\min_{\boldsymbol{\beta}} f(\boldsymbol{\beta}) = \frac{1}{M} \sum_{i=1}^M (x_1^i(\boldsymbol{\beta}) - r_0)^2, \quad (5.5)$$

where  $\boldsymbol{\beta} = \{\beta_1, \dots, \beta_5\}$  and  $M$  refers to the number of nodes on the free surface of the final product (which can vary in between optimization iterations). The simulation parameters used in this design problem are tabulated in Table 1. The tolerance used in the thermal sensitivity analysis to decide the nature of the boundary conditions is taken as  $1.00 \times 10^{-5}$ . A straight (flat) die is chosen as the initial (guess) preforming die.

The steepest descent method with optimal step size selection is used to perform the optimization. The variation of the objective function with the iteration index is shown in Fig. 8. Results show that convergence is achieved in about 12 iterations. Fig. 9 shows the initial, intermediate and optimal solution of the preforming die shape for the thermo-mechanical design problem of minimizing barreling after the finishing stage.

Table 1  
Simulation parameters for 2 stage open die forging of Al 1100-O at 673 K (Example 1)

| Parameter                                      | Value                 |
|--|-----------------------|
| Energy error norm                              | $1.00 \times 10^{-6}$ |
| Displacement $L_2$ error norm                  | $1.00 \times 10^{-6}$ |
| Normal penalty in direct contact problem       | $1.00 \times 10^{+5}$ |
| Tangent penalty in direct contact problem      | $1.00 \times 10^{+4}$ |
| Normal penalty in sensitivity contact problem  | $1.00 \times 10^{+7}$ |
| Tangent penalty in sensitivity contact problem | $1.00 \times 10^{+5}$ |
| Tolerance for gap                              | $1.00 \times 10^{-5}$ |
| Tolerance for slip                             | $1.00 \times 10^{-5}$ |
| Tolerance for convergence in thermal problem   | $1.00 \times 10^{-4}$ |

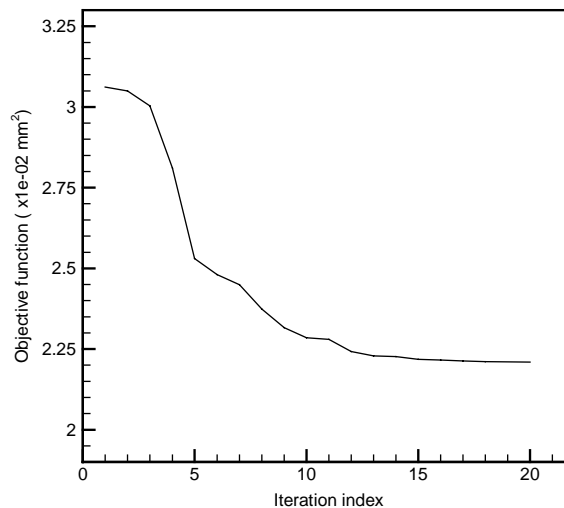


Fig 8. Variation of the objective function which quantifies the amount of barreling in the final product versus the optimization iteration index (Example 1).

### 5.2. Preform design for closed-die forging–fill die cavity and achieve uniform state distribution (Example 2)

In this example, the design of the preforming die shape is addressed so as to achieve a distribution of the state variable in the final product obtained after the finishing stage that is as uniform as possible. The initial workpiece in the preforming stage is fixed and is a right circular cylinder of radius  $r = 0.85$  mm and height 2.4 mm. The height reduction at  $r = 0$ , in the first stage is 1.2 mm and in the second stage is 0.6 mm. The friction coefficient, initial temperature and other thermal data are kept the same as in the earlier example.

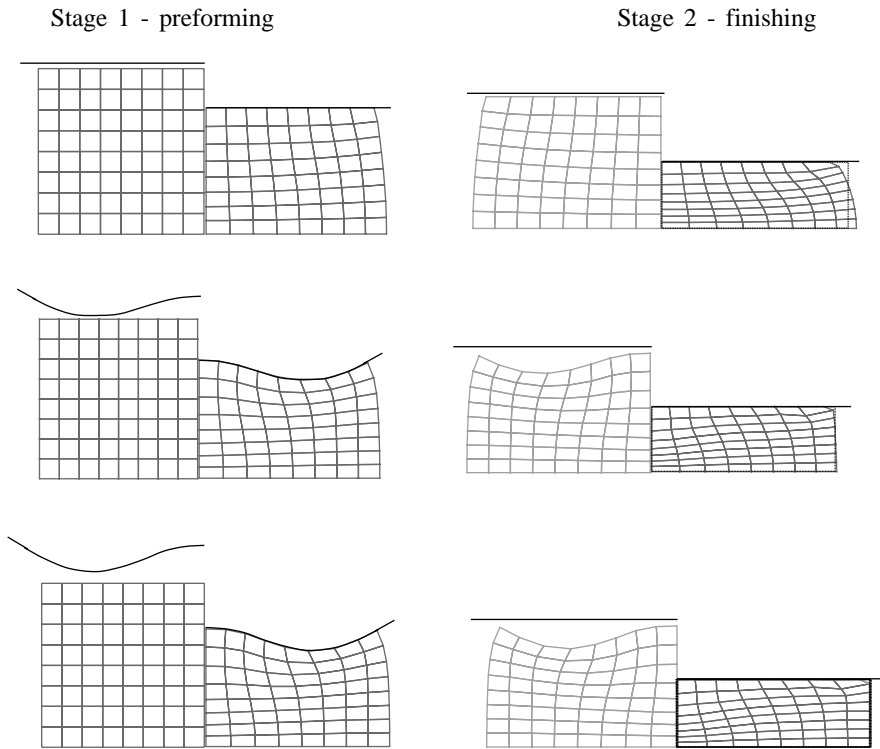


Fig 9. Optimal solution for the thermo-mechanical preform forging design problem minimizing barreling (Example 1).

The preforming die (contact) surface  $R_{\beta}(\alpha)$  is represented in the same way as in the earlier example. The finishing die surface is defined as follows ( $\eta \in [0, 1]$ ):

$$\text{shape}(\eta) = \begin{cases} r(\eta) = 1.3 * (1 - \eta) \\ z(\eta) = \begin{cases} 1.3 + 10.58 * \eta - 62.43 * \eta^2 + 122.8 * \eta^3, & \eta \in [0.00, 0.17], \\ 1.9, & \eta \in [0.17, 0.37], \\ 3.1 - 11.9 * \eta + 44.38 * \eta^2 - 76.8 * \eta^3, \\ \quad + 60.5 * \eta^{4.0} - 17.7 * \eta^5, & \eta \in [0.37, 1.0]. \end{cases} \end{cases}$$

The finite dimensional optimization problem is now posed as follows:

$$\min_{\beta} f(\beta) = \frac{\omega_1}{M} \sum_{i=1}^M (s_i(\beta) - \bar{s}(\beta))^2, \tag{5.6}$$

where  $M$  is here defined as the total number of sampling points in the volume and  $\bar{s}$  is the resulting average value of the state variable. The factor  $\omega_1 = 6.25 \times 10^{-4} \text{ MPa}^{-2}$  is introduced to non-dimensionalize the cost functional and is obtained from the solution of a reference single-stage problem for which the mean state variable obtained is 40 MPa.

Table 2  
Simulation parameters for closed die forging of Al 1100-O at 673 K (Example 2)

| Parameter                                      | Value                 |
|--|-----------------------|
| Energy error norm                              | $1.00 \times 10^{-4}$ |
| Displacement $L_2$ error norm                  | $1.00 \times 10^{-4}$ |
| Normal penalty in direct contact problem       | $1.00 \times 10^{+5}$ |
| Tangent penalty in direct contact problem      | $1.00 \times 10^{+4}$ |
| Normal penalty in sensitivity contact problem  | $1.00 \times 10^{+8}$ |
| Tangent penalty in sensitivity contact problem | $1.00 \times 10^{+7}$ |
| Tolerance for gap                              | $1.00 \times 10^{-5}$ |
| Tolerance for slip                             | $1.00 \times 10^{-4}$ |
| Tolerance for friction                         | $1.00 \times 10^{-4}$ |
| Tolerance for convergence in thermal problem   | $1.00 \times 10^{-4}$ |

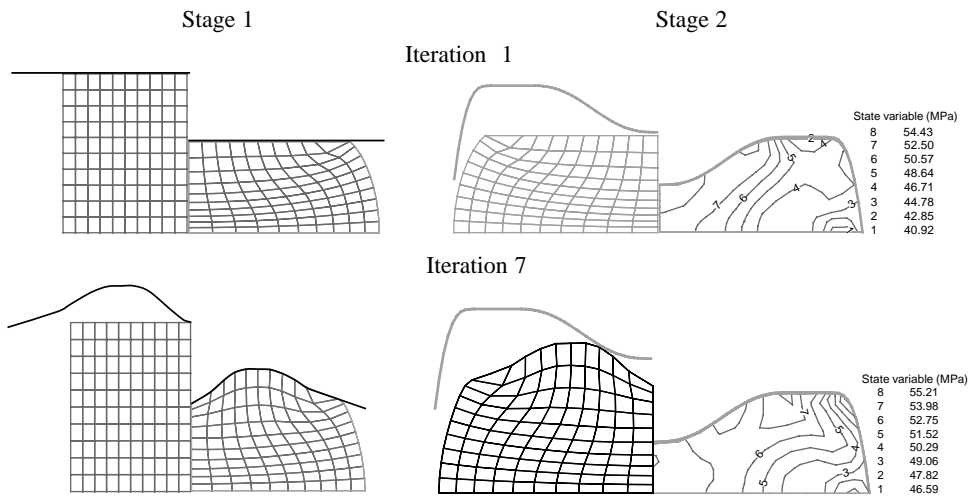


Fig 10. Comparison of the final product obtained using the initial and optimal solution for the thermo-mechanical preform forging design problem (Example 2).

The steepest descent method with optimal step size selection is used in this example as well. The simulation parameters used in this example are tabulated in Table 2. The tolerance used in the thermal sensitivity analysis to decide the nature of the boundary conditions is taken as  $1.00 \times 10^{-5}$ . The initial preforming die shape is chosen to be flat.

The products obtained using the initial preforming die shape and the final (i.e. optimal) solution are shown in Fig. 10. The average value and the deviation of the material state in the initial product were computed as 50.2 and 3.73 MPa, respectively. The corresponding values in the optimum product are 52.3 MPa and 1.88 MPa, respectively. Fig. 11 gives the variation of the objective function with iterations. The change in the preforming die shape with iterations is presented in Fig. 12.

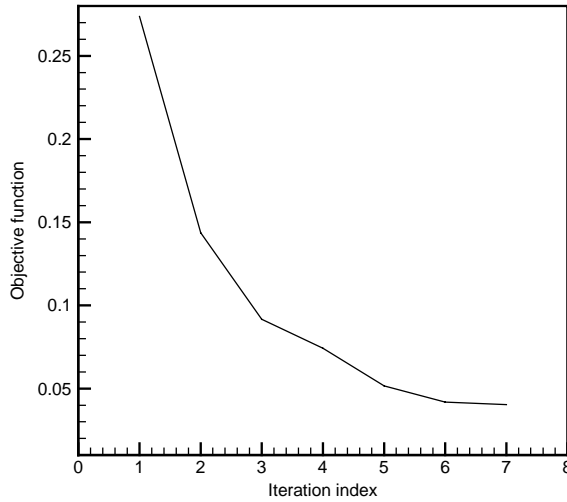


Fig 11. Variation of the objective function with optimization iterations (Example 2).

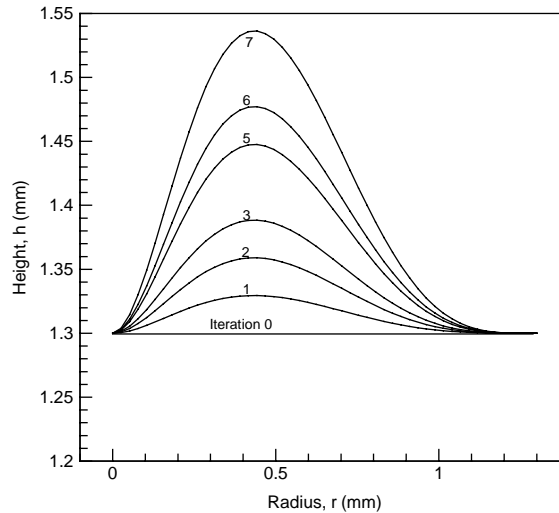


Fig 12. Variation of the preforming die shape with optimization iterations (Example 2).

### 5.3. Two-stage isothermal forging process design for manufacturing of an engine disk (Example 3)

This example presents a forging process design for producing an axisymmetric ribbed disk. The initial billet is a right cylinder of 2 mm height and 0.88 mm radius. The height reduction at  $r = 0$ , in the first stage is 0.9 mm and in the second stage is 0.5 mm. A quarter of the billet is modelled in the simulation and design. The friction coefficient in the preforming stage is taken as 0.2 and in the finishing stage as 0.1. For simplicity of the design process, isothermal process conditions (673 K) are assumed herein.

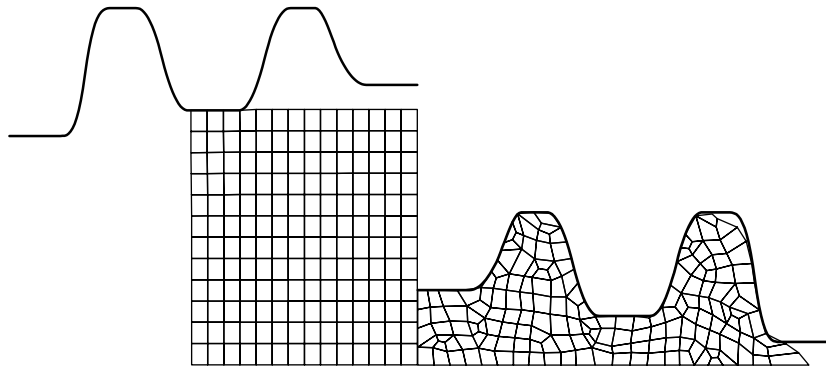


Fig 13. Reference one-stage design using a right-circular cylinder of the required volume (Example 3).

The finishing die is defined as follows:

$$\text{shape}(\eta) = \begin{cases} r(\eta) = 1.6 * (1 - \eta), \\ z(\eta) = \begin{cases} 0.8, & \eta \in [0.00, 0.12], \\ 1100 * (\eta - 0.125)^3 + 0.80, & \eta \in [0.12, 0.19], \\ 946 * (\eta - 0.25)^3 + 1.30, & \eta \in [0.19, 0.25], \\ 1.30, & \eta \in [0.25, 0.31], \\ -3.70 + 32.00 * \eta - 51.20 * \eta^2, & \eta \in [0.31, 0.38], \\ 10.70 - 44.80 * \eta + 51.20 * \eta^2, & \eta \in [0.38, 0.44], \\ 0.90, & \eta \in [0.44, 0.56], \\ 17.10 - 57.60 * \eta + 51.20 * \eta^2, & \eta \in [0.56, 0.62], \\ -22.90 + 70.40 * \eta + 51.20 * \eta^2, & \eta \in [0.62, 0.69], \\ 1.30, & \eta \in [0.69, 0.75], \\ -402. + 1536 * \eta - 1945 * \eta^2 + 819 * \eta^3, & \eta \in [0.75, 0.81], \\ 20.60 - 44.80 * \eta + 25.60 * \eta^2, & \eta \in [0.81, 0.87], \\ 1.00, & \eta \in [0.87, 1.00], \end{cases} \end{cases}$$

where  $\eta \in [0, 1]$ .

All tolerances are the same as in Example 1 except for the frictional tolerance of gap that is taken as  $10^{-4}$ . The tangent and normal penalty numbers in the sensitivity problem are here taken as  $10^7$  and  $10^8$ , respectively. The average number of remeshings during the optimization iterations was none for the first stage and 8 for the second stage.

When a single stage process is considered (using a right-circular cylinder of the fixed required volume of  $4.93 \text{ mm}^3$ ), one can notice from Fig. 13 that the die cavity cannot be filled in the upper-right corner. To overcome this problem, a possible solution will be to start with considerably

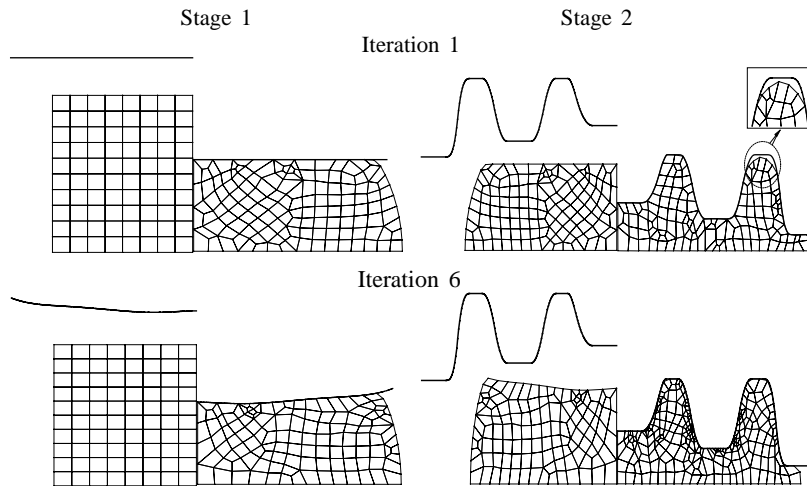


Fig. 14. Comparison of the final product obtained using the initial and optimal solution for the thermo-mechanical preform forging design problem (Example 3).

more material than that required. However, this could lead to a high forging force and sizeable increase in flash. An alternative solution to this problem is to design a multi-stage process, in which the initial billet (right circular cylinder) is preformed to some intermediate shape. This preform is then formed to the desired shape using the finishing die. The solution reported has demonstrated that the design intent of the final product can be achieved with a two-stage process. The design example is thus re-posed as a two-stage design problem, where an open die is adopted in the performing stage and a closed die in the finishing stage. In the design process, the closed die is kept unchanged to form the desired boundary of the final product and the objective is to design the open die shape such that the finishing die cavity can be completely filled:

$$\min_{\beta} f(\beta) = \frac{1}{M} \sum_{i=1}^M ((x^i(\beta) - x^d)^2 + (y^i(\beta) - y^d)^2), \quad (5.7)$$

where  $M$  is the total number of nodes on the contact surface of the final product (which varies with optimization iterations) and  $(x^d, y^d)$  defines the desired boundary of the final product (which here is the nearest location on the die). The BFGS algorithm is used to solve the above optimization problem.

Fig. 14 shows the design process of the performing die. When an initial guess (flat die) is used, a noticeable gap appears at the top of the outer cavity. After only 4 iterations, the die cavity was completely filled. The convergence is plotted in Fig. 15 and the preforming dies obtained during the optimization iterations are presented in Fig. 16.

Finally, a comparison of the force histories for the reference (non-optimized) one-stage design process and the two-stage optimal process computed using the CSM method is provided in Fig. 17. Even though, the objective of the simulation was to solely control the shape in the final product, it is apparent that, as byproduct of the design simulation, a reduction in the maximum force was obtained as well.

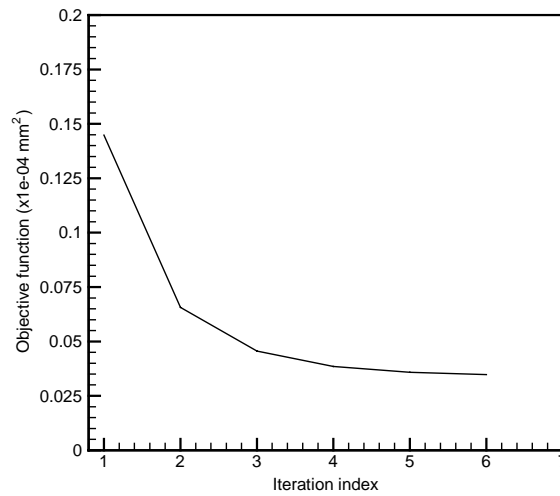


Fig 15. Convergence index for design optimization problem (Example 3).

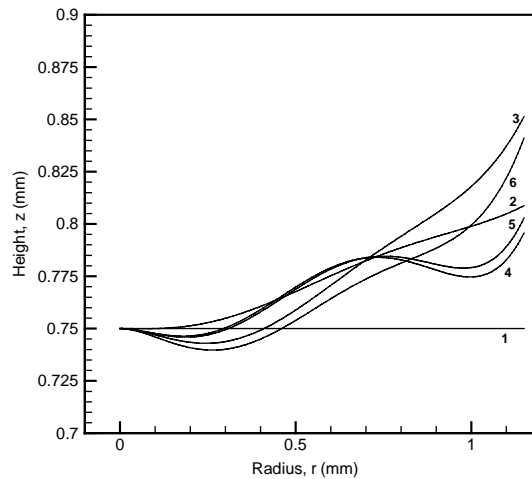


Fig 16. Preforming die shapes obtained during the optimization process (Example 3).

## 6. Conclusions

Through this paper, we have developed a novel updated Lagrangian framework for large deformation sensitivity analysis of multi-stage processes that yields very accurate estimates of design sensitivities even after several remeshing operations have been performed during the analysis. The developed continuum sensitivity analysis can be used to design industrial multi-stage deformation processes. It allows control of the product properties and microstructure by proper process sequence selection and design of mechanical and thermal process parameters. The industrial relevance of the developed simulator was demonstrated with a variety of practical multi-stage forming design

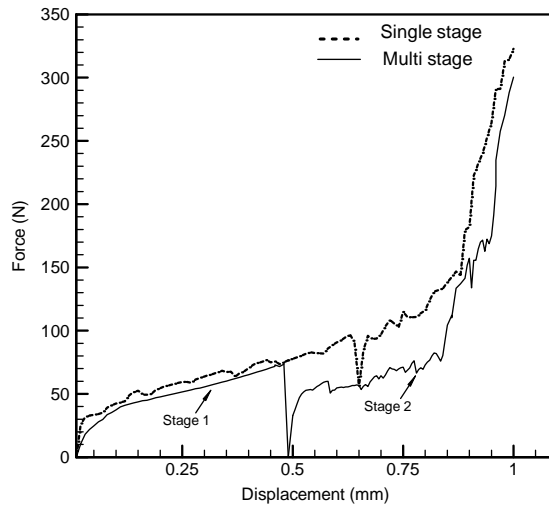


Fig 17. A comparison of the required forging force histories for the one-stage reference design and the two-stage optimal design (Example 3).

applications. The presented simulator can enhance the design of industrial processes and result in an increased reliability and affordability. Further developments in this direction are needed including 3D-implementations, consideration of purely thermal stages, development of algorithms for initial designs and others. This research effort can lead to a virtual process laboratory that will assist industry in reducing lead time for process development, in trimming the cost of an extensive experimental trial-and-error process development effort, in developing processes for tailored material properties and in increasing volume/time yield.

### Acknowledgements

The work presented here was funded by the Computational Mathematics program of the Air Force Office of Scientific Research (grant F49620-00-1-0373), by the Air Force Research Laboratory (grants TMC96-5835-0018-09-05 and TMC98-5835-0018-15) and by the National Science Foundation (grant DMI-0113295). Additional support was provided by the Materials Process Design Group of the Alcoa Technical Center (Dr. Paul Wang, program leader). The computing for this project was supported by the Cornell Theory Center. The authors would also like to thank Dr. Srikanth Akkaram of General Electric-CRD for his various technical contributions in the earlier stages of this work.

### References

- [1] Kobayashi S, Oh S, Altan T. *Metal forming and the finite element method*. New York: Oxford University Press, 1989.
- [2] Tortorelli DA, Michaleris P. Design sensitivity analysis: overview and review. *Inverse Problems in Engineering* 1994;1:71–105.

- [3] Tsay JJ, Arora JS. Nonlinear structural design sensitivity analysis for path dependent problems. Part 1: general theory. *Computer Methods in Applied Mechanics and Engineering* 1990;81:183–208.
- [4] Badrinarayanan S, Zabarás N. A sensitivity analysis for the optimal design of metal forming processes. *Computer Methods in Applied Mechanics and Engineering* 1996;129:319–48.
- [5] Fourment L, Chenot JL. Optimal design for non-steady state metal forming processes—I. shape optimization method. *International Journal for Numerical Methods in Engineering* 1996;39:33–50.
- [6] Fourment L, Balan T, Chenot JL. Optimal design for non-steady state metal forming processes—II. application of shape optimization in forging. *International Journal for Numerical Methods in Engineering* 1996;39:51–65.
- [7] Noor AK, Needleman A, Peters JM. Sensitivity analysis for failure and damage in dynamically loaded tensile bars. *Computer Methods in Applied Mechanics and Engineering* 1998;151:461–78.
- [8] Antúnez HJ. Thermo-mechanical modeling and sensitivity analysis for metal forming operations. *Computer Methods in Applied Mechanics and Engineering* 1998;161:113–25.
- [9] Kowalczyk P, Kleiber M. Shape sensitivity in elasto-plastic computations. *Computer Methods in Applied Mechanics and Engineering* 1999;171:371–86.
- [10] Zhao G, Wright E, Grandhi RV. Preform die shape design in metal forming using an optimization method. *International Journal for Numerical Methods in Engineering* 1997;40:1213–30.
- [11] Joun MS, Hwang SM. Die shape optimal design in three dimensional shape metal extrusion by the finite element method. *International Journal for Numerical Methods in Engineering* 1998;41:311–35.
- [12] Chung SH, Hwang SM. Optimal process design in non-isothermal non-steady metal forming by the finite element method. *International Journal for Numerical Methods in Engineering* 1998;42:1343–90.
- [13] Gao ZY, Grandhi RV. Sensitivity analysis and shape optimization for preform design in thermo-mechanical coupled analysis. *International Journal for Numerical Methods in Engineering* 1999;45:1349–73.
- [14] Byon SM, Hwang SM. Process optimal design in non-isothermal steady-state metal forming by the finite element method. *International Journal for Numerical Methods in Engineering* 1999;46:1075–100.
- [15] Doltsinis I, Rodic T. Process design and sensitivity analysis in metal forming. *International Journal for Numerical Methods in Engineering* 1999;45:661–92.
- [16] Feng JP, Luo ZJ. A method for the optimal control of forging process variables using the finite element method and control theory. *Journal of Materials Processing Technology* 2000;108:40–4.
- [17] Kim HS, Im YT. Multi-stage cold forging process design with a searching algorithm. *Transactions of NAMRI/SME* 1996;24:161–6.
- [18] Chung K, Richmond O. Ideal Forming—I: homogeneous deformation with minimum plastic work. *International Journal of Mechanical Sciences* 1992;34(7):575–91.
- [19] Chung K, Richmond O. Ideal Forming—II: sheet forming with optimum deformation. *International Journal of Mechanical Sciences* 1992;34(8):617–33.
- [20] Roy S, Ghosh S, Shivpuri R. Optimal design of process variables in multi-pass wire drawing by genetic algorithms. *Journal of Manufacturing Science and Engineering* 1996;118:244–51.
- [21] Chung JS, Hwang SM. Application of a genetic algorithm to the optimal design of the die shape in extrusion. *Journal of Materials Processing Technology* 1998;72:69–77.
- [22] Chung JS, Hwang SM. Application of a genetic algorithm to process optimal design in non-isothermal metal forming. *Journal of Materials Processing Technology* 1998;80-81:136–43.
- [23] Kim H, Altan T, Sevenler K. Computer aided part and processing sequence design in cold forging. *Journal of Material Processing Technology* 1992;33:57–74.
- [24] Badrinarayanan S, Constantinescu A, Zabarás N. Preform design in metal forming. In: Shen S-F, Dawson P, editors. *Numerical methods in industrial forming processes*. Rotterdam: Balkema, 1995. p. 533–8.
- [25] Zabarás N, Bao Y, Srikanth A, Frazier WG. A continuum Lagrangian sensitivity analysis for metal forming processes with applications to die design problems. *International Journal for Numerical Methods in Engineering* 2000;48: 679–720.
- [26] Srikanth A, Zabarás N. Shape optimization and preform design in metal forming processes. *Computer Methods in Applied Mechanics and Engineering* 2000;190:1859–901.
- [27] Srikanth A, Zabarás N. A gradient based optimization approach for the design of single and multi-stage metal forming processes. In: Furness RJ, editor. *ASME Publ., MED Vol-11*, 2000. p. 495–507.

- [28] Srikanth A, Zabaras N. A computational model for the finite element analysis of thermoplasticity with ductile damage at finite strains. *International Journal for Numerical Methods in Engineering* 1999;45:1569–605.
- [29] Weber G, Anand L. Finite deformation constitutive equations and a time integration procedure for isotropic, hyperelastic–viscoplastic solids. *Computer Methods in Applied Mechanics and Engineering* 1990;79:173–202.
- [30] Zabaras N, Srikanth A. An object oriented programming approach to the Lagrangian FEM analysis of large inelastic deformations and metal forming processes. *International Journal for Numerical Methods in Engineering* 1999;45:399–445.
- [31] Laursen TA, Simo JC. On the formulation and numerical treatment of finite deformation frictional contact problems. In: Wriggers P, Wager W, editors. *Nonlinear computational mechanics-state of the art*. Berlin: Springer, 1991. p. 716–36.
- [32] Srikanth A, Zabaras N. Using objects to model finite deformation plasticity. *Engineering With Computers* 1999;15:37–60.
- [33] Srikanth A, Zabaras N. An updated Lagrangian finite element sensitivity analysis of large deformations using quadrilateral elements. *International Journal for Numerical Methods in Engineering* 2001;52:1131–63.
- [34] de Souza Neto EA, Perić D, Dutko M, Owen DRJ. Design of simple low order finite elements for large strain analysis of nearly incompressible solids. *International Journal of Solids and Structures* 1996;33:3277–96.
- [35] Ganapathysubramanian S, Zabaras N. A continuum sensitivity method for finite thermo-inelastic deformations with applications to the design of hot forming processes. *International Journal for Numerical Methods in Engineering* 2002;55:1391–437.
- [36] Brown SB, Kim KH, Anand L. An internal variable constitutive model for hot working of metals. *International Journal of Plasticity* 1989;5:95–130.